VOLUME 112, NUMBER 15
JULY 18, 1990

JOURNAL
OF THE
AMERICAN
CHEMICAL
SOCIETY

Chiral Discrimination in Electronic Energy-Transfer Processes between Dissymmetric Metal Complexes in Solution. Time-Resolved Chiroptical Luminescence Measurements of Enantioselective Excited-State Quenching Kinetics

David H. Metcalf,*,† Seth W. Snyder,‡ J. N. Demas,† and F. S. Richardson*,†

Contribution from the Chemistry Department and Biophysics Program, University of Virginia, Charlottesville, Virginia 22901. *Received January 16, 1990*

Abstract: Steady-state and time-resolved chiroptical luminescence measurements are used to investigate enantioselective excited-state quenching processes in solution. Theory and measurement methodology are presented for the case in which an initially *racemic* excited-state population of chiral luminophores evolves to a *nonracemic* population in the presence of chiral quencher molecules. Generation of enantiomeric excess in the luminophore excited-state population produces differential (spontaneous) emission of left and right circularly polarized light, and the time dependence of this *chiroptical luminescence* provides a direct measure of the differential excited-state quenching kinetics associated with homochiral versus heterochiral luminophore–quencher interactions. Experimental results are presented for a series of systems in which the luminophores are dissymmetric, tris(terdentate) lanthanide complexes and the quenchers are dissymmetric, tris(bidentate) transition-metal complexes. Each of the lanthanide and transition-metal complexes has trigonal-dihedral (D_3) symmetry, but the complexes differ with respect to their electronic state structures, spectroscopic properties, and ligand sizes and shapes. These differences in structural and spectroscopic properties are reflected in the quenching rate parameters measured for different luminophore–quencher (Q) combinations, and they have a particularly strong influence on the differential rate parameters associated with enantioselective (homochiral versus heterochiral) quenching. Lanthanide excited-state (Ln*) quenching in these systems occurs via an electronic energy-transfer (Ln* to Q) mechanism, and enantioselective quenching reflects chiral discrimination in the intermolecular interactions that govern energy-transfer probabilities. The quenching results are interpreted within the framework of a phenomenological model for energy transfer via an electron-exchange mechanism, and enantioselectivity in the quenching is attributed to (1) structural differences between the collisional complexes formed by homochiral versus heterochiral diastereomeric donor (Ln*)–acceptor (Q) pairs and/or (2) chiral discrimination in the purely electronic interactions *directly* responsible for energy transfer (i.e., chirality dependence in the electron-exchange integrals). Our results indicate that *both* 1 and 2 contribute to the enantioselective quenching kinetics observed for the Ln*–Q systems and that the respective contributions may be either additive or subtractive.

Chirality-dependent interactions between molecules and chiral recognition in chemical and physical processes are of significant interest and importance in chemistry and biology. Chiral recognition is manifested in a wide variety of chemical processes occurring in nature, and it is exploited extensively in laboratory syntheses and separations of complex chemical systems. Chiral recognition in both chemical and physical processes has been studied for many years, and significant progress has been made in developing empirical correlations between molecular stereochemical structure, environmental and bulk-medium properties, and the degree of chiral recognition observed in a given process. For many systems and processes, these correlations can be rationalized satisfactorily in terms of intermolecular *contact* interactions and the molecular stereochemical properties that govern these interactions. In other cases, however, chiral recognition

* To whom correspondence should be addressed.
† Chemistry Department.
‡ Biophysics Program. Present address: Chemistry Division, Argonne National Laboratory, Argonne, IL 60439.

0002-7863/90/1512-5681$02.50/0

appears to occur over distances that are larger than molecular dimensions, and chiral discrimination in longer range (noncontact) interaction mechanisms must be considered.

Considerable attention has been given to the fundamental nature of chirality-dependent interactions between molecules, and formal theory in this area is reasonably well-developed.[1-14] The theoretical formulations identify the principal interaction mechanisms expected to contribute to chiral discrimination under various conditions (defined with respect to intrinsic molecular properties, relative molecular orientations, and intermolecular distances), and they provide prescriptions for calculating interaction energy differentials for homochiral versus heterochiral pairs of molecular enantiomers. These formulations have been of significant heuristic value for rationalizing chiral discrimination and recognition in terms of qualitative structural and mechanistic considerations, but quantitative calculations based on them have met with only limited success. In most systems and processes of practical interest, the chiral discriminatory interactions represent only a small fraction of the total intermolecular interaction energy, multiple interaction mechanisms are likely to make important contributions, and environmental effects can be substantial. It is not surprising, therefore, that detailed mechanistic analyses and quantitative calculations of chiral discriminatory properties have proved to be difficult. More quantitative experimental characterizations of these properties in reasonably well-defined systems (and processes) are needed to improve our mechanistic understanding of chiral recognition phenomena *and* to narrow the gap between qualitative, phenomenological interpretive models and fundamental theory.

Chiral recognition in photochemical and photophysical processes has been the subject of numerous studies reported in the literature, and particular attention has been given to enantioselectivity in photoinduced electron-transfer reactions *and* to the differential formation (and stability) of homochiral versus heterochiral exciplex species.[15] In the present study, we examine chiral discrimination in electronic energy-transfer processes between dissymmetric lanthanide and transition-metal complexes in aqueous solution. The complexes chosen for study have well-defined structures, and their spectroscopic properties are well-characterized. In our experiments, the lanthanide complexes (Ln) function as luminophores whose luminescence can be quenched by the transition-metal complexes (Q). The structures of the lanthanide and transition-metal complexes have trigonal-dihedral (D_3) symmetry and exist as optical isomers (enantiomers) with either left-handed (Λ) or right-handed (Δ) configurational chirality about the trigonal symmetry axis. The solution samples examined in our experiments contain *resolved* transition-metal complexes (either ΛQ or ΔQ) and a *racemic* mixture of lanthanide complexes (*rac*-Ln). The lanthanide complexes are excited with a pulse of unpolarized light, and the lanthanide luminescence is then monitored for chiroptical activity as a function of time. The measured quantities are $I = I_l + I_r$, $\Delta I = I_l - I_r$, and $g_{em} = 2\Delta I/I$, where I_l and I_r denote, respectively, left and right circularly polarized intensity components in the luminescence and g_{em} is commonly called an emission dissymmetry factor.[16-18] Both the circularly polarized intensity differential (ΔI) and the emission dissymmetry factor (g_{em}) provide measures of chiroptical activity in the emitting-state population of the lanthanide complexes, and nonvanishing values obtained for these quantities are diagnostic of a *nonracemic* emitting-state population. Furthermore, the sign and magnitude of g_{em} may be correlated with the enantiomeric excess in this population.

Excitation of *rac*-Ln with unpolarized light produces a racemic excited-state population of complexes (*rac*-Ln*), and in the absence of chiral perturbations this population will remain racemic during its entire lifetime. However, in the presence of chiral quencher molecules (say, ΛQ), it is possible that the Λ and Δ enantiomers of Ln* will be differentially quenched and the initially prepared racemic excited-state population will become nonracemic. Enantiomeric excess in the excited state will grow at a rate that depends on the difference in rate constants for ΛLn*–ΛQ versus ΔLn*–ΛQ quenching actions. If the rate of this quencher-induced excited-state resolution process is comparable to the rate of luminescence decay (of Ln* in the presence of Q), the rate of formation of enantiomeric excess in the emitting-state population may be determined from time-resolved measurements of the emission dissymmetry factor g_{em}. Combining these measurements of $g_{em}(t)$ with measurements of $I(t)$ and $\Delta I(t)$, one may determine the sum, difference, and ratio of rate constants associated with *homochiral*, ΛLn*–ΛQ, and *heterochiral*, ΔLn*–ΛQ, quenching. Denoting these respective rate constants as $k_q^{\Lambda\Lambda}$ and $k_q^{\Delta\Lambda}$, the ratio $(k_q^{\Lambda\Lambda} - k_q^{\Delta\Lambda})/(k_q^{\Lambda\Lambda} + k_q^{\Delta\Lambda})$ provides a convenient measure of enantioselectivity in the quenching processes. The sign of this ratio differentiates between preferential homochiral versus heterochiral quenching, and its magnitude reflects the degree of chiral discrimination present in the quenching mechanisms.

In a previous communication,[19] we reported enantioselective luminescence quenching results for $Tb(dpa)_3^{3-}$ (dpa ≡ dipicolinate dianion ≡ 2,6-pyridinedicarboxylate) in neutral aqueous solution with $Ru(phen)_3^{2+}$ (phen ≡ 1,10-phenanthroline). Both the nine-coordinate, tris(terdentate) $Tb(dpa)_3^{3-}$ complexes and the six-coordinate, tris(bidentate) $Ru(phen)_3^{2+}$ complexes have dissymmetric structures of D_3 point-group symmetry in which the metal–ligand chelate rings form a three-bladed propeller with either left-handed (Λ) or right-handed (Δ) helicity about the trigonal symmetry axis. Our solution samples contained *racemic* $Tb(dpa)_3^{3-}$ (10 or 15 mM) and *resolved* Λ(or Δ)-$Ru(phen)_3^{2+}$, with [Ru]/[Tb] ratios ranging from 3×10^{-4} to 1.5×10^{-2}. The $Tb(dpa)_3^{3-}$ complexes were excited with unpolarized light, and terbium luminescence was analyzed for chiroptical activity under both steady-state excitation/emission–detection conditions *and* pulsed-excitation/time-resolved emission–detection conditions. The time-resolved measurements showed that chiroptical activity was absent in the luminescence observed at early times in the detection cycle but that chiroptical activity was generated over the remaining lifetime of the terbium excited-state population. These results

(1) Mason, S. F. *Molecular Optical Activity and the Chiral Discriminations*; Cambridge University Press: Cambridge, 1982.
(2) Mavroyannis, C.; Stephen, M. J. *Mol. Phys.* **1962**, *5*, 629–638.
(3) Chang, T. Y. *Int. J. Quantum Chem.* **1971**, *5*, 469–473.
(4) Craig, D. P.; Power, E. A.; Thirunamachandran, T. *Proc. R. Soc. London* **1971**, *A322*, 165–179.
(5) Dissado, L. A. *J. Phys. C: Solid State Phys.* **1974**, *7*, 463–480.
(6) Craig, D. P.; Schipper, P. E. *Proc. R. Soc. London* **1975**, *A342*, 19–37.
(7) Craig, D. P.; Radom, L.; Stiles, P. J. *Proc. R. Soc. London* **1975**, *A343*, 11–16.
(8) Craig, D. P.; Mellor, D. P. *Topics Curr. Chem.* **1976**, *63*, 1–48.
(9) Schipper, P. E. *Chem. Phys.* **1977**, *26*, 29–34.
(10) (a) Craig, D. P. In *Optical Activity and Chiral Discrimination*; Mason, S. F., Ed.; Reidel: Dordrecht, 1979; Chapter 12, pp 293–318. (b) Mason, S. F. *Ibid.*, Chapter 13, pp 319–337.
(11) (a) Kuroda, R.; Mason, S. F.; Rodger, C. D.; Seal, R. H. *Chem. Phys. Lett.* **1978**, *57*, 1–4. (b) Kuroda, R.; Mason, S. F.; Rodger, C. D.; Seal, R. H. *Mol. Phys.* **1981**, *42*, 33–50.
(12) Chiu, Y. N.; Kenny, A. V.; Brown, S. H. *J. Chem. Phys.* **1980**, *73*, 1422–1431.
(13) Craig, D. P.; Thirunamachandran, T. *Molecular Quantum Electrodynamics*; Academic Press: London, 1984; Chapter 7, pp 142–182.
(14) Schipper, P. E. *Aust. J. Chem.* **1982**, *35*, 1513–1524.
(15) For examples, see: Avnir, D.; Wellner, E.; Ottolenghi, M. *J. Am. Chem. Soc.* **1989**, *111*, 2001–2003. Joshi, V.; Ghosh, P. K. *J. Am. Chem. Soc.* **1989**, *111*, 5604–5612. Ohkubo, K.; Hamada, T.; Inaoka, T.; Ishida, H. *Inorg. Chem.* **1989**, *28*, 2021–2022. Lopez-Arbeloa, F.; Van Der Auweraer, M.; Ruttens, F.; De Schryver, F. C. *J. Photochem. Photobiol.* **1988**, *44*, 63–83. Lopez-Arbeloa, F.; Goedeweeck, R.; Andriessen, R.; De Schryver, F. C. *J. Photochem. Photobiol.* **1988**, *42*, 133–148. Lopez-Arbeloa, F.; Goedeweeck, R.; Ruttens, F.; De Schryver, F. C.; Sisado, M. *J. Am. Chem. Soc.* **1987**, *109*, 3068–3076. Thomas, M. P.; Patonay, G.; Warner, I. M. *Anal. Lett.* **1987**, *20*, 717–730. Kano, K.; Matsumoto, H.; Hashimoto, S.; Sisido, M.; Imanishi, Y. *J. Am. Chem. Soc.* **1985**, *107*, 6117–6118. Rau, H. *Chem. Rev.* **1983**, *83*, 535–547. Yorozu, T.; Hayashi, K.; Irie, M. *J. Am. Chem. Soc.* **1981**, *103*, 5480–5484. Tran, C. D.; Fendler, J. H. *J. Am. Chem. Soc.* **1980**, *102*, 2923–2928. Gafni, A. *J. Am. Chem. Soc.* **1980**, *102*, 7367–7368. Brittain, H.; Ambrozich, D. L.; Saburi, M.; Fendler, J. H. *J. Am. Chem. Soc.* **1980**, *102*, 6372–6374. Tundo, P.; Fendler, J. H. *J. Am. Chem. Soc.* **1980**, *102*, 1760–1762. Porter, G. B.; Sparks, R. H. *J. Photochem.* **1980**, *13*, 123–131. Porter, G. B.; Sparks, R. H. *J. Chem. Soc., Chem. Commun.* **1979**, 1094–1095. Brittain, H. G. *Inorg. Chem.* **1979**, *18*, 1740–1745.
(16) Richardson, F. S. *J. Less-Common Met.* **1989**, *149*, 161–177.
(17) Riehl, J. P.; Richardson, F. S. *Chem. Rev.* **1986**, *86*, 1–16.
(18) Richardson, F. S.; Riehl, J. P. *Chem. Rev.* **1977**, *77*, 773–791.
(19) Metcalf, D. H.; Snyder, S. W.; Wu, S.; Hilmes, G. L.; Riehl, J. P.; Demas, J. N.; Richardson, F. S. *J. Am. Chem. Soc.* **1989**, *111*, 3082–3083.

reflect the generation of enantiomeric excess in an excited-state population that starts out as racemic, and this was attributed to differential quenching of Λ-$Tb(dpa)_3^{3-}$ versus Δ-$Tb(dpa)_3^{3-}$ excited-state complexes by chiral Λ(or Δ)-$Ru(phen)_3^{2+}$. A detailed analysis of the quenching kinetics was not given, but it was estimated that the rate constants for homochiral versus heterochiral quenching processes differed by a factor of 2. Furthermore, results obtained as a function of [Ru]/[Tb] concentration ratios indicated that a single Ru complex can be involved in multiple quenching events during the lifetime of the terbium excited-state population.

The enantioselective luminescence quenching results reported in ref 19 (and cited above) were not analyzed in detail, and they do not provide an adequate basis for detailed mechanistic interpretation. However, they support several *general* conclusions that can provide useful working hypotheses for more detailed studies. First, chiral discrimination in the interactions between ground-state Tb and Ru complexes is too weak to produce a racemic to nonracemic shift in the equilibrium population of Λ-Tb and Δ-Tb enantiomers. This conclusion is supported by the following results: (1) No circular dichroism (CD) is observed in the absorptive transitions of the Tb complexes, and (2) no chiroptical activity is observed in the early luminescence of Tb* complexes excited with unpolarized light. Both of these observations are diagnostic of a racemic ground-state population of Tb complexes. Second, terbium luminescence derives entirely from discrete, structurally intact $Tb(dpa)_3^{3-}$ complexes, with no evidence for contributions from other terbium complexes (including Tb*–Ru exciplexes). Third, a single Ru complex may quench many Tb* complexes during the lifetime of the terbium excited-state population, and these quenching actions exhibit an enantioselectivity that provides evidence for chiral discrimination in the quenching mechanisms. The electronic state structures and spectroscopic properties of the $Tb(dpa)_3^{3-}$ and $Ru(phen)_3^{2+}$ complexes are quite compatible with a quenching mechanism in which Tb* to Ru electronic energy transfer occurs *and* in which individual ruthenium complexes can be repetitively recycled as energy-transfer acceptor species. The emissive transitions of $Tb(dpa)_3^{3-}$ have significant spectral overlap with absorptive transitions in $Ru(phen)_3^{2+}$, and excited-state lifetimes in $Ru(phen)_3^{2+}$ are significantly shorter than the luminescence lifetime of $Tb(dpa)_3^{3-}$ (by at least 3 orders of magnitude for the states relevant to the energy-transfer mechanism). The relatively fast excited to ground state decay rates for the $Ru(phen)_3^{2+}$ complexes make these complexes available for multiple quenching actions.

In this paper, we present theory and methods of analysis that are relevant to chiroptical luminescence studies of enantioselective excited-state quenching processes, we present new results and analyses for these processes in the $Tb(dpa)_3^{3-}$–$Ru(phen)_3^{2+}$ system, and we report results obtained for several additional luminophore–quencher systems comprised of lanthanide (Ln) and transition-metal (Q) complexes in aqueous solution. The lanthanide complexes are either $Tb(dpa)_3^{3-}$ or $Eu(dpa)_3^{3-}$, and the transition-metal (quencher) complexes include resolved (Λ or Δ) $Ru(phen)_3^{2+}$, $Co(phen)_3^{3+}$, $Ru(bpy)_3^{2+}$, and $Co(en)_3^{3+}$ (where bpy ≡ 2,2′-bipyridine and en ≡ 1,2-diaminoethane ≡ ethylenediamine). All of these species have trigonal-dihedral (D_3) symmetry, the $Tb(dpa)_3^{3-}$ and $Eu(dpa)_3^{3-}$ complexes have essentially identical coordination geometries, and the only significant structural differences among the transition-metal complexes are in the relative sizes and shapes of the ligands (see Figure 1 for depictions of metal–ligand chelate rings in the respective complexes and Figure 2 for full structural representations of the complexes). However, the Tb and Eu complexes have significantly different electronic state structures and spectroscopic properties (for electronic processes occurring primarily within the $4f^N$ electronic configuration), and the Ru and Co complexes differ with respect to their net charge (+2 versus +3) and their electronic excited-state structure and properties. The differences in spectroscopic and electronic excited-state properties influence the relative energy-transfer probabilities for the different types of Ln (donor)–Q (acceptor) pairs, and this is reflected in the quenching results obtained for the different Ln–Q pair combinations. Differences in the

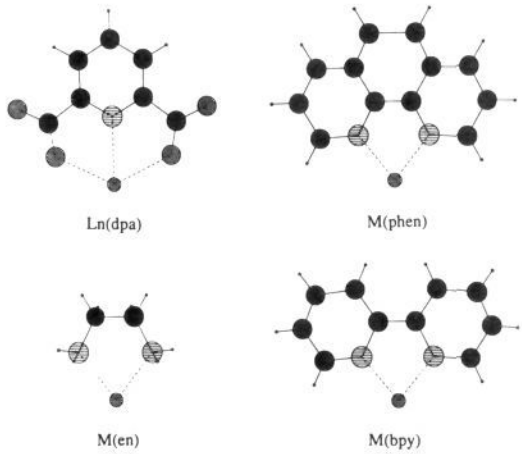

Figure 1. Metal–*single* ligand chelate structures for the lanthanide (Ln ≡ Tb^{3+} or Eu^{3+}) and transition-metal (M ≡ Ru^{2+} or Co^{3+}) complexes: ⊕ ≡ metal atom, ⊖ ≡ nitrogen atom, ⊗ ≡ oxygen atom, ● ≡ carbon atom, ○ ≡ hydrogen atom.

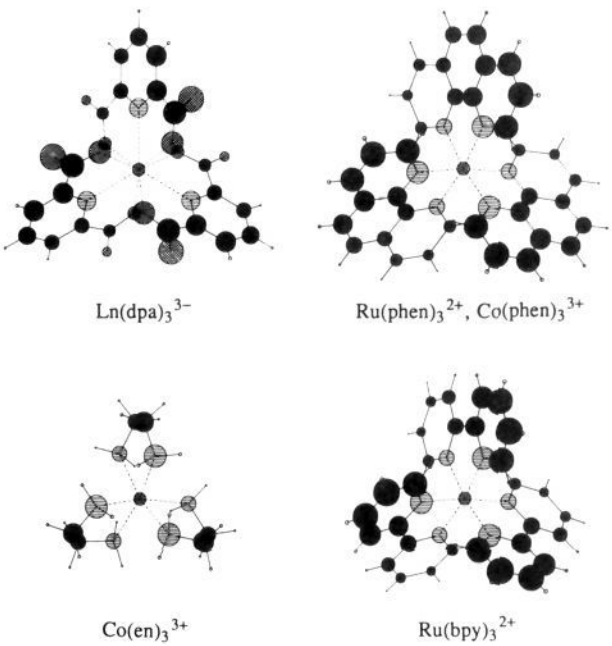

Figure 2. Full structural representations of the tris(terdentate) lanthanide and tris(*bidentate*) transition-metal complexes, viewed along the trigonal (C_3) symmetry axis. Atom types are depicted as in Figure 1.

quenching results obtained for Tb–Q versus Eu–Q systems can be explained entirely in terms of relative electronic excited-state properties of the Tb, Eu, and Q complexes. However, quenching results obtained for a given Ln with different quencher complexes indicate that ligand size and shape, as well as electronic excited-state properties, have an influence on quenching efficiency and kinetics. This ligand influence is particularly apparent in the quenching parameters associated with enantioselectivity, which suggests that chiral discrimination in the quenching processes occurs primarily via short-range interactions. It is important to note, however, that even when the Ln and Q complexes are in van der Waals contact, the metal ions will remain separated by at least 8–12 Å in the systems examined here.

Circularly polarized luminescence (CPL) spectroscopy provides a direct probe of excited-state chiroptical activity in molecules, and *steady-state* CPL measurements have been reported for a wide variety of luminescent systems over the past 20 years.[16-18,20,21]

(20) Steinberg, I. Z. *Annu. Rev. Biophys. Bioeng.* **1978**, *7*, 113–137.
(21) Brittain, H. G. In *Molecular Luminescence Spectroscopy: Methods and Applications*; Schulman, S. G., Ed.; Wiley: New York, 1985; pp 583–620.

Time-resolved circularly polarized luminescence (TR-CPL) measurements have been reported only recently,[19,22] and they have proved valuable in investigations of dynamic molecular properties and processes that depend on chirality. In the present study, TR-CPL measurements provide the decisive evidence for intermolecular chiral discrimination in dynamic excited-state quenching processes, and they are used to determine the kinetic parameters that characterize these processes. The TR-CPL technique is a uniquely suitable probe for the types of processes examined in this study.

Theory and Measurement Methodology

In this section we present theory, formulate expressions, and describe measurement methodology relevant to chiroptical luminescence studies of enantioselective excited-state quenching kinetics. The theory is developed in terms of phenomenological rate laws for spectroscopic and electronic excited-state quenching processes in solution samples that contain chiral luminescent molecules and chiral quenching species. The theory yields rate parameters that reflect the relative probabilities of homochiral and heterochiral quenching, and it relates these parameters to the rate at which a racemic excited-state population of luminophores becomes nonracemic (and exhibits chiroptical luminescence) in the presence of a nonracemic mixture of chiral quencher molecules. Furthermore, relationships between these parameters and the chiroptical luminescence observables are derived, and measurement techniques are discussed in a general context. The formulations presented in this section are largely phenomenological, and they do not address the mechanistic origins of chiral discrimination in enantioselective excited-state quenching processes.

The *general* methodologies employed in this study are applicable to a much broader class of luminophore–quencher systems than is represented by the lanthanide and transition-metal complexes described in the introduction. However, the treatment that follows is tailored to the types of systems and experimental conditions represented in the current study. It is assumed that (1) the luminophore and quencher species each exist in only two structural forms that are optical antipodes (enantiomers); (2) quenching occurs via a bimolecular mechanism involving diastereomeric pairs of luminophore and quencher enantiomers; (3) luminescence from isolated (unperturbed) luminophores can be distinguished from quencher and exciplex luminescence; and (4) both the ground- and emitting-state populations of species are isotropic with respect to the spatial and orientational distributions of luminophores and quenchers. The last-mentioned condition (4) is of particular importance for the chiroptical luminescence measurements employed in this study. In our experiments we use solution samples in which the luminophores are excited with unpolarized light and have rotational diffusion rates that are fast compared to excited-state decay rates.

Kinetic Model and Rate Expressions. In the expressions that follow, we use the same generic notation that was used in the introduction for specifying enantiomers of the lanthanide luminophore complexes (ΛLn and ΔLn) and enantiomers of the transition-metal quencher complexes (ΛQ and ΔQ). Asterisks are used to denote electronic excited-state species, and square brackets denote species concentration. Enantiomeric excess in the *ground-state* quencher population is defined by

$$\eta_Q = \frac{[\Lambda Q] - [\Delta Q]}{[Q]} \qquad (1)$$

where $[Q] = [\Lambda Q] + [\Delta Q]$ and enantiomeric excess in the lanthanide *excited-state* population is defined by

$$\eta_{Ln^*} = \frac{[\Lambda Ln^*] - [\Delta Ln^*]}{[Ln^*]} \qquad (2)$$

where $[Ln^*] = [\Lambda Ln^*] + [\Delta Ln^*]$.

The following processes are considered in our kinetic model:

(a) excitation of *rac*-Ln with unpolarized light

$$\Lambda Ln + h\nu \rightarrow \Lambda Ln^* \qquad k_{exc}^{\Lambda}$$

$$\Delta Ln + h\nu \rightarrow \Delta Ln^* \qquad k_{exc}^{\Delta}$$

(b) decay of Ln* complexes in the absence of quencher (Q) actions

$$\Lambda Ln^* \rightarrow \Lambda Ln + h\nu' + \text{nonradiative energy} \qquad k_0^{\Lambda}$$

$$\Delta Ln^* \rightarrow \Delta Ln + h\nu' + \text{nonradiative energy} \qquad k_0^{\Delta}$$

(c) deexcitation of Ln* complexes by quencher species

$$\Lambda Ln^* + \Lambda Q \rightarrow \Lambda Ln + \Lambda Q^* \qquad k_q^{\Lambda\Lambda}$$

$$\Lambda Ln^* + \Delta Q \rightarrow \Lambda Ln + \Delta Q^* \qquad k_q^{\Lambda\Delta}$$

$$\Delta Ln^* + \Lambda Q \rightarrow \Delta Ln + \Lambda Q^* \qquad k_q^{\Delta\Lambda}$$

$$\Delta Ln^* + \Delta Q \rightarrow \Delta Ln + \Delta Q^* \qquad k_q^{\Delta\Delta}$$

(d) interconversions of ΛLn* and ΔLn* enantiomers

$$\Lambda Ln^* \rightarrow \Delta Ln^* \qquad k_{conv}^{\Lambda}$$

$$\Delta Ln^* \rightarrow \Lambda Ln^* \qquad k_{conv}^{\Delta}$$

The processes shown in d reflect enantiomer interconversions that might occur in stereochemically labile Ln* systems. Among the ten rate constants shown above, there are five pairwise identities and we can reduce the number of unique rate constants to five: $k_{exc} \equiv k_{exc}^{\Lambda} = k_{exc}^{\Delta}$; $k_0 \equiv k_0^{\Lambda} = k_0^{\Delta}$; $k_q^{\Lambda\Lambda} = k_q^{\Delta\Delta}$; $k_q^{\Lambda\Delta} = k_q^{\Delta\Lambda}$; $k_{conv} \equiv k_{conv}^{\Lambda} = k_{conv}^{\Delta}$. These relations will be used in developing rate law expressions.

The rate laws of interest are those showing the rates at which the ΛLn* and ΔLn* excited-state populations decay after their preparation with a pulse of unpolarized light. On the basis of the processes shown above, the appropriate differential rate expressions may be written as

$$\frac{-d[\Lambda Ln^*]}{dt} = (k_0 + k_q^{\Lambda\Lambda}[\Lambda Q] + k_q^{\Lambda\Delta}[\Delta Q])[\Lambda Ln^*] + k_{conv}([\Lambda Ln^*] - [\Delta Ln^*]) \qquad (3)$$

$$\frac{-d[\Delta Ln^*]}{dt} = (k_0 + k_q^{\Delta\Lambda}[\Lambda Q] + k_q^{\Delta\Delta}[\Delta Q])[\Delta Ln^*] - k_{conv}([\Lambda Ln^*] - [\Delta Ln^*]) \qquad (4)$$

In a previous study,[22] we measured k_{conv} and k_0 for $Eu(dpa)_3^{3-}$ in H_2O at a series of temperatures between 293.2 and 353.2 K. At 293.2 K, we obtained the values $k_{conv} = 15.8\ s^{-1}$ and $k_0 = 619.7\ s^{-1}$; and at 353.2 K, we obtained the values $k_{conv} = 449.8\ s^{-1}$ and $k_0 = 634.6\ s^{-1}$. At all temperatures below 315 K, the ratio of k_{conv} to k_0 was determined to be less than 0.1, and at 293.2 K, this ratio is 0.025. We expect the enantiomer interconversion kinetics for $Tb(dpa)_3^{3-}$ to be virtually identical with those of $Eu(dpa)_3^{3-}$, since the mechanism for racemization is entirely chemical, rather than involving electronic states of the lanthanide ion. For $Tb(dpa)_3^{3-}$ in H_2O, the value of k_0 is $469.5\ s^{-1}$ at 293.2 K and we estimate a value of 0.034 for the ratio of k_{conv} to k_0. These data suggest that enantiomer interconversion processes will not make a significant contribution to the experimental observations reported in the present study, and the k_{conv}-dependent terms in eqs 3 and 4 may be neglected. In other words, it can be assumed that the luminescence decay rates for the excited $Eu(dpa)_3^{3-}$ and $Tb(dpa)_3^{3-}$ complexes are much faster than the enantiomer interconversion rates. Making this assumption, eqs 3 and 4 may be reexpressed as follows:

$$\frac{-d[\Lambda Ln^*]}{[\Lambda Ln^*]} = (k_0 + k_q^{\Lambda\Lambda}[\Lambda Q] + k_q^{\Lambda\Delta}[\Delta Q])\,dt \qquad (5)$$

$$\frac{-d[\Delta Ln^*]}{[\Delta Ln^*]} = (k_0 + k_q^{\Delta\Lambda}[\Lambda Q] + k_q^{\Delta\Delta}[\Delta Q])\,dt \qquad (6)$$

Under the conditions employed in our experiments, the transition-metal (quencher) complexes are nonlabile with respect to

(22) Metcalf, D. H.; Snyder, S. W.; Demas, J. N.; Richardson, F. S. *J. Am. Chem. Soc.* **1990**, *112*, 469–479.

enantiomer interconversion and their excited-state lifetimes are short compared to the time intervals within which we measure Ln* luminescence (vide infra). Therefore, we may assume that the relative *and* absolute concentrations of ΛQ and ΔQ remain essentially constant throughout our measurement periods. Given this assumption, eqs 5 and 6 may be integrated to obtain

$$[\Lambda Ln^*]^t = [\Lambda Ln^*]^0 e^{(-k_0 - k_q^{\Lambda\Lambda}[\Lambda Q] - k_q^{\Delta\Lambda}[\Delta Q])t} \quad (7)$$

$$[\Delta Ln^*]^t = [\Delta Ln^*]^0 e^{(-k_0 - k_q^{\Lambda\Delta}[\Lambda Q] - k_q^{\Delta\Delta}[\Delta Q])t} \quad (8)$$

where the superscripts of $[\Lambda Ln^*]^t$ and $[\Delta Ln^*]^t$ denote time after excitation and it is assumed that $[\Lambda Q] = [\Lambda Q]^0 = [\Lambda Q]^t$ (and similarly for [ΔQ]). For an initially *racemic* population of Ln* complexes, $[\Lambda Ln^*]^0 = [\Delta Ln^*]^0$, the ratio of $[\Lambda Ln^*]^t$ to $[\Delta Ln^*]^t$ may be written as

$$\frac{[\Lambda Ln^*]^t}{[\Delta Ln^*]^t} = e^{(k_q^{\Lambda\Lambda} - k_q^{\Lambda\Delta})\eta_Q[Q]t} \quad (9)$$

where $\eta_Q[Q]$ is defined according to eq 1 and we have made use of the relations $k_q^{\Delta\Delta} = k_q^{\Lambda\Lambda}$ and $k_q^{\Lambda\Delta} = k_q^{\Delta\Lambda}$. This ratio is related to enantiomeric excess in the Ln* population according to

$$\frac{[\Lambda Ln^*]^t}{[\Delta Ln^*]^t} = \frac{1 + \eta^t_{Ln^*}}{1 - \eta^t_{Ln^*}} \quad (10)$$

where $\eta^t_{Ln^*}$ is defined according to eq 2. Combining eqs 9 and 10 yields the following expressions for the time evolution of enantiomeric excess in the Ln* population

$$\eta^t_{Ln^*} = \frac{e^{k_d\eta_Q[Q]t/2} - e^{-k_d\eta_Q[Q]t/2}}{e^{k_d\eta_Q[Q]t/2} + e^{-k_d\eta_Q[Q]t/2}} \quad (11a)$$

$$\eta^t_{Ln^*} = \tanh\left(\frac{k_d\eta_Q[Q]t}{2}\right) \quad (11b)$$

where $k_d = k_q^{\Delta\Lambda} - k_q^{\Lambda\Lambda}$ and tanh denotes a hyperbolic tangent function.

It is useful here to introduce two additional parameters defined by

$$k_q = (k_q^{\Lambda\Lambda} + k_q^{\Delta\Lambda})/2 \quad (12)$$

$$E_q = \frac{(k_q^{\Lambda\Lambda} - k_q^{\Delta\Lambda})}{(k_q^{\Lambda\Lambda} + k_q^{\Delta\Lambda})} = \frac{-k_d}{2k_q} \quad (13)$$

The parameter k_q corresponds to the quenching rate constant that would be measured for a sample that is racemic with respect to both the Ln* *and* Q species. The parameter E_q provides a measure of the degree of enantioselectivity in the quenching of *rac*-Ln* by a fully resolved (Λ or Δ) quencher population. Expressed in terms of k_q and E_q, eq 11b may be rewritten as

$$\eta^t_{Ln^*} = \tanh(-k_q E_q \eta_Q[Q]t) \quad (14)$$

The E_q parameter can have values ranging from +1 (corresponding to purely *homochiral* quenching) to −1 (corresponding to purely *heterochiral* quenching). Finally, we note that the ratio of $k_q^{\Lambda\Lambda}$ to $k_q^{\Delta\Lambda}$ is related to k_q, k_d, and E_q according to

$$\frac{k_q^{\Lambda\Lambda}}{k_q^{\Delta\Lambda}} = \frac{2k_q - k_d}{2k_q + k_d} = \frac{1 + E_q}{1 - E_q} \quad (15)$$

Time-Resolved Chiroptical Luminescence Measurements. The following quantities are measured in the chiroptical luminescence experiments

$$I(\lambda',t) = I_l(\lambda',t) + I_r(\lambda',t) \quad (16)$$

$$\Delta I(\lambda',t) = I_l(\lambda',t) - I_r(\lambda',t) \quad (17)$$

$$g_{em}(\lambda',t) = \frac{2\Delta I(\lambda',t)}{I(\lambda',t)} \quad (18)$$

where λ′ denotes emission wavelength and I_l and I_r denote intensities for the left and right circularly polarized components of the sample luminescence. Following previous practice, we refer to I as a *total luminescence* (TL) intensity, we refer to ΔI as a *circularly polarized luminescence* (CPL) intensity, and we call g_{em} an *emission dissymmetry factor*.[17] The magnitudes of both I and ΔI depend on luminophore concentration, excitation intensity, and emission collection and detection efficiency, whereas the measured values of g_{em} are independent of these factors. Opposite enantiomers of a chiral luminophore will give identical TL signals, and they will give CPL signals that are equal in magnitude but opposite in sign. For a sample that contains a mixture of luminophore enantiomers characterized by a *fixed* (time-independent) enantiomeric excess, the emission dissymmetry factor is given by

$$g_{em}(\lambda') = \eta g^{\Lambda}_{em}(\lambda') = -\eta g^{\Delta}_{em}(\lambda') \quad (19)$$

where η denotes enantiomeric excess in the emitting-state population of luminophores and $g^{\Lambda}_{em}(\lambda')$ and $g^{\Delta}_{em}(\lambda')$ are emission dissymmetry factors characteristic of completely *resolved* Λ and Δ enantiomers. In this case, the TL and CPL intensities will exhibit the *same* time dependence, and g_{em} will be time-independent. However, if enantiomeric excess *varies* during the luminescence lifetime of the sample, the TL and CPL intensities will exhibit *different* time-dependent behavior and g_{em} will reflect, directly, the time-dependent variations in enantiomeric excess.

$$g_{em}(\lambda',t) = \eta^t g^{\Lambda}_{em}(\lambda') = -\eta^t g^{\Delta}_{em}(\lambda') \quad (20)$$

In the preceding section of this paper, we derived an expression for the enantiomeric excess generated in an initially racemic excited-state population of dissymmetric luminophores (Ln*) by enantioselective quenching processes (see eq 11b). That expression can be used in eq 20 if *either* of the following conditions are met: (1) The emitting state is excited directly, or (2) the emitting-state population is formed from higher excited states via relaxation processes that are fast compared to quenching processes. Either one of these two conditions can be satisfied for the systems and experiments described in the present study, and eqs 11b and 20 may be combined to obtain

$$g_{em}(\lambda',t) = g^{\Lambda}_{em}(\lambda') \tanh\left(\frac{k_d\eta_Q[Q]t}{2}\right) \quad (21)$$

Alternatively, eqs 14 and 20 may be combined to obtain

$$g_{em}(\lambda',t) = g^{\Lambda}_{em}(\lambda') \tanh(-k_q E_q \eta_Q[Q]t) \quad (22)$$

For a sample that contains a mixture of ΛLn* and ΔLn* luminophores, the total luminescence expression (16) may be rewritten as

$$I(\lambda',t) = I_l^{\Lambda}(\lambda',t) + I_l^{\Delta}(\lambda',t) + I_r^{\Lambda}(\lambda',t) + I_r^{\Delta}(\lambda',t) \quad (23)$$

where the left (l) and right (r) circularly polarized intensity contributions made by the ΛLn* and ΔLn* species are identified separately. Each term in eq 23 may be related to a luminophore concentration according to $I_l^{\Lambda}(\lambda',t) = K_l^{\Lambda}(\lambda')[\Lambda Ln^*]^t$, $I_l^{\Delta}(\lambda',t) = K_l^{\Delta}(\lambda')[\Delta Ln^*]^t$, $I_r^{\Lambda}(\lambda',t) = K_r^{\Lambda}(\lambda')[\Lambda Ln^*]^t$, and $I_r^{\Delta}(\lambda',t) = K_r^{\Delta}(\lambda')[\Delta Ln^*]^t$, where the K quantities are defined to include spontaneous emission probabilities for left or right circularly polarized emission at wavelength λ′ by ΛLn* and ΔLn*. Among the K quantities, we have the identities $K_l^{\Lambda}(\lambda') = K_r^{\Delta}(\lambda')$ and $K_r^{\Lambda}(\lambda') = K_l^{\Delta}(\lambda')$. Using these identities, we can rewrite eq 23 as

$$I(\lambda',t) = [K_l^{\Lambda}(\lambda') + K_r^{\Lambda}(\lambda')]([\Lambda Ln^*]^t + [\Delta Ln^*]^t) \quad (24)$$

Expressions for $[\Lambda Ln^*]^t$ and $[\Delta Ln^*]^t$ were derived earlier in the paper for the case in which ΛLn* and ΔLn* are subject to enantioselective quenching by nonracemic quencher species (Q). The relevant expressions are (7) and (8), and we combine them with eq 24 to obtain

$$I(\lambda',t) = [K_l^{\Lambda}(\lambda') + K_r^{\Lambda}(\lambda')] \times ([\Lambda Ln^*]^0 e^{(-k_0 - k_q^{\Lambda\Lambda}[\Lambda Q] - k_q^{\Delta\Lambda}[\Delta Q])t} + [\Delta Ln^*]^0 e^{(-k_0 - k_q^{\Lambda\Delta}[\Lambda Q] - k_q^{\Delta\Delta}[\Delta Q])t}) \quad (25)$$

In the experiments of interest here, the emitting-state population of Ln* is *initially* racemic and we have $[\Lambda Ln^*]^0 = [\Delta Ln^*]^0 = {}^1/_2[Ln^*]^0$. This condition permits eq 25 to be reduced to the form

$$I(\lambda',t) = {}^1/_2 I(\lambda',0)e^{-(k_0+k_q[Q])t}[e^{k_d\eta_Q[Q]t/2} + e^{-k_d\eta_Q[Q]t/2}] \quad (26)$$

where $k_q = (k_q^{\Delta\Delta} + k_q^{\Lambda\Lambda})/2$, $k_d = (k_q^{\Delta\Delta} - k_q^{\Lambda\Lambda})$, $[Q] = [\Lambda Q] + [\Delta Q]$, η_Q is defined according to eq 1, and

$$I(\lambda',0) = [K_l^{\Lambda}(\lambda') + K_r^{\Lambda}(\lambda')][Ln^*]^0 \quad (27)$$

Expressions analogous to (23) and (24) may be written for CPL intensity:

$$\Delta I(\lambda',t) = I_l^{\Lambda}(\lambda',t) + I_l^{\Delta}(\lambda',t) - I_r^{\Lambda}(\lambda',t) - I_r^{\Delta}(\lambda',t) \quad (28a)$$

$$\Delta I(\lambda',t) = [K_l^{\Lambda}(\lambda') - K_r^{\Lambda}(\lambda')]([\Lambda Ln^*]^t - [\Delta Ln^*]^t) \quad (28b)$$

The latter expression (28b) may be further developed to the form

$$\Delta I(\lambda',t) = {}^1/_2[K_l^{\Lambda}(\lambda') - K_r^{\Lambda}(\lambda')][Ln^*]^0 e^{-(k_0+k_q[Q])t}[e^{k_d\eta_Q[Q]t/2} - e^{-k_d\eta_Q[Q]t/2}] \quad (29)$$

The emission dissymmetry factor for *pure* ΛLn* enantiomers is given by

$$g_{em}^{\Lambda}(\lambda') = \frac{2[I_l^{\Lambda}(\lambda') - I_r^{\Lambda}(\lambda')]}{I_l^{\Lambda}(\lambda') + I_r^{\Lambda}(\lambda')} = \frac{2[K_l^{\Lambda}(\lambda') - K_r^{\Lambda}(\lambda')]}{K_l^{\Lambda}(\lambda') + K_r^{\Lambda}(\lambda')} \quad (30)$$

and from eq 27 we note that

$$K_l^{\Lambda}(\lambda') + K_r^{\Lambda}(\lambda') = \frac{I(\lambda',0)}{[Ln^*]^0} \quad (31)$$

Therefore, we have the relationship

$${}^1/_2 g_{em}^{\Lambda}(\lambda')\, I(\lambda',0) = [K_l^{\Lambda}(\lambda') - K_r^{\Lambda}(\lambda')][Ln^*]^0 \quad (32)$$

which may be used in eq 29 to obtain

$$\Delta I(\lambda',t) = {}^1/_4 g_{em}^{\Lambda}(\lambda')\, I(\lambda',0)e^{-(k_0+k_q[Q])t}[e^{k_d\eta_Q[Q]t/2} - e^{-k_d\eta_Q[Q]t/2}] \quad (33)$$

If we divide eq 33 by eq 26 and then multiply by 2, we obtain

$$\frac{2\Delta I(\lambda',t)}{I(\lambda',t)} = g_{em}^{\Lambda}(\lambda')\frac{e^{k_d\eta_Q[Q]t/2} - e^{-k_d\eta_Q[Q]t/2}}{e^{k_d\eta_Q[Q]t/2} + e^{-k_d\eta_Q[Q]t/2}} \quad (34a)$$

$$\frac{2\Delta I(\lambda',t)}{I(\lambda',t)} = g_{em}^{\Lambda}(\lambda')\tanh\left(\frac{k_d\eta_Q[Q]t}{2}\right) \quad (34b)$$

which is the time-dependent emission dissymmetry factor generated by enantioselective quenching.

Expressions 26 and 33 for $I(\lambda',t)$ and $\Delta I(\lambda',t)$, respectively, each contain three rate parameters, k_0, k_q, and k_d. Two of these parameters, k_0 and k_q, can be characterized completely from time-resolved measurements of $I(\lambda',t)$ at a series of *racemic* quencher concentrations ($\eta_Q = 0$). In principle, the magnitude (but *not* the sign) of the k_d parameter may also be determined from $I(\lambda',t)$ measurements when the quencher concentration is *nonracemic* ($\eta_Q \neq 0$). In this latter case, the time dependence of $I(\lambda',t)$ can exhibit double-exponential behavior characterized by decay rate constants expressed as $-(k_0 + k_q[Q] \pm k_d\eta_Q[Q]/2)$ or, equivalently, $-(k_0 + k_q[Q] \mp k_qE_q\eta_Q[Q])$. If we consider the *optimal* case in which $\eta_Q = \pm 1$ (fully resolved quencher) and $E_q = \pm 1$ (maximum enantioselectivity in quenching actions), the final term in the last expression will be $\mp k_q[Q]$. For the systems examined in the present study, the values of $k_q[Q]$ were generally in the range of 100–1000 s^{-1}. Double exponentiality in $I(\lambda',t)$ data may arise from other sources (multiple quenching species, for example), and so the unequivocal determination of k_d (or E_q) parameters from analyses of $I(\lambda',t)$ data can be difficult.

Emission dissymmetry factor measurements provide a *direct* means for determining both the magnitude *and* sign of the k_d rate parameter in cases where either $g_{em}^{\Lambda}(\lambda')$ or $g_{em}^{\Delta}(\lambda')$ is known for the luminophore (see eqs 20 and 21). Measurements of $g_{em}^{\Lambda}(\lambda')$ or $g_{em}^{\Delta}(\lambda')$ require an enantiomerically pure (fully resolved) sample of luminophores. Many chiral luminophores of general interest can be chemically resolved, their isolated enantiomers are stable with respect to racemization (in both their ground and excited states), and their $g_{em}^{\Lambda}(\lambda') = -g_{em}^{\Delta}(\lambda')$ values can be measured. However, the luminophores examined in the present study are stereochemically labile in both their ground and excited states (characterized by racemization rate constants of ca. 32 s^{-1} at 20 °C),[22] and their $g_{em}^{\Lambda}(\lambda')$ and $g_{em}^{\Delta}(\lambda')$ values cannot be measured directly. Without knowledge of $g_{em}^{\Lambda}(\lambda')$, values of k_d can only be determined from emission dissymmetry factor measurements by performing fits of $g_{em}(\lambda',t)$ data to eq 21, with the use of $g_{em}^{\Lambda}(\lambda')$ and k_d as fitting parameters. These fits are aided by the tight bounds on $g_{em}^{\Lambda}(\lambda')$ values (restricted to the range of +2 to −2), and they yield magnitudes and *relative* signs for the k_d and $g_{em}^{\Lambda}(\lambda')$ parameters. However, the *absolute* signs of these parameters cannot be determined from the fits.

Steady-State Chiroptical Luminescence Measurements. Time-resolved measurements are essential for obtaining a complete characterization of enantioselective quenching kinetics, but steady-state measurements (which are somewhat easier to perform) can provide useful confirmatory tests of the parameters derived from the time-resolved measurements. In the steady-state experiments, the sample is irradiated continuously with unpolarized light and both the TL intensity (I) and the CPL intensity (ΔI) are measured as a function of emission wavelength λ′. Expressions for the *steady-state* quantities $\bar{I}(\lambda')$ and $\overline{\Delta I}(\lambda')$ are readily obtained from integrations of eqs 26 and 33 over time, and the steady-state emission dissymmetry factor is given by

$$\bar{g}_{em}(\lambda') = \frac{2\overline{\Delta I}(\lambda')}{\bar{I}(\lambda')} = g_{em}^{\Lambda}(\lambda')\left[\frac{k_d\eta_Q[Q]/2}{k_0 + k_q[Q]}\right] \quad (35a)$$

$$\bar{g}_{em}(\lambda') = g_{em}^{\Lambda}(\lambda')\left[\frac{-E_qk_q\eta_Q[Q]}{k_0 + k_q[Q]}\right] \quad (35b)$$

Expressed in terms of luminescence lifetime parameters, eq 35b may be written as

$$\bar{g}_{em}(\lambda') = -g_{em}^{\Lambda}(\lambda')E_q\eta_Q[1 - (\tau_{[Q]}/\tau_0)] \quad (36)$$

where $\tau_0 = k_0^{-1}$ (the lifetime of Ln* in the absence of quencher) and $\tau_{[Q]} = (k_0 + k_q[Q])^{-1}$ (the lifetime of Ln* in the presence of a *racemic* quencher concentration [Q]).

The steady-state enantiomeric excess produced in the Ln* population is given by

$$\bar{\eta}_{Ln^*} = \frac{k_d\eta_Q[Q]/2}{k_0 + k_q[Q]} \quad (37a)$$

$$\bar{\eta}_{Ln^*} = \frac{-E_qk_q\eta_Q[Q]}{k_0 + k_q[Q]} \quad (37b)$$

For the *limiting* case in which $\eta_Q = \pm 1$ (completely resolved quencher) and $E_q = \pm 1$ (completely homochiral or heterochiral quenching), the magnitude of $\bar{\eta}_{Ln^*}$ is given by

$$\lim_{\eta_Q=\pm1, E_q=\pm1} |\bar{\eta}_{Ln^*}| = 1 - (\tau_{[Q]}/\tau_0) \quad (38)$$

and the limiting magnitude of $\bar{g}_{em}(\lambda')$ is

$$\lim |\bar{g}_{em}(\lambda')| = |g_{em}^{\Lambda}(\lambda')|[1 - (\tau_{[Q]}/\tau_0)] \quad (39)$$

Excitation and Emission Properties of Complexes

$Tb(dpa)_3^{3-}$. Luminescence spectra of $Tb(dpa)_3^{3-}$ complexes in neutral aqueous solution may be assigned to transitions originating from crystal field levels split out of the $^5D_4$ multiplet of the $4f^8(Tb^{3+})$ electronic configuration. The baricenter of this multiplet is located approximately 20 370 cm^{-1} above the baricenter of the $^7F_6$ *ground* multiplet of $4f^8(Tb^{3+})$, and a $^5D_4$ luminescence spectrum exhibits seven distinct transition regions that may be assigned to $^7F_J \leftarrow {}^5D_4$ ($J = 0$–6) multiplet to multiplet transition manifolds. The most intense emission lines occur in the $^7F_5 \leftarrow {}^5D_4$ transition region, and this region also exhibits relatively strong chiroptical properties (CPL and emission dissymmetry factors).

The $^7F_5 \leftarrow {}^5D_4$ luminescence spans the 535–555-nm wavelength range, and chiroptical properties measured within this spectral region are used in the present study.

In this study, terbium $^5D_4$ luminescence was excited with laser radiation at *either* 488 nm *or* 325 nm. Radiation of 488-nm wavelength excites the $^5D_4$ multiplet *directly*, whereas 325-nm radiation excites ligand levels that populate $^5D_4$ via nonradiative, ligand to terbium energy-transfer processes. Absorption at 325 nm is several orders of magnitude stronger than absorption at 488 nm, but the photostability and luminescence properties of Tb(dpa)$_3^{3-}$ are essentially the same for 325 nm versus 488 nm excitation. On the other hand, photostability among the transition-metal (quencher) complexes employed in this study exhibits some sensitivity to irradiation wavelength (vide infra).

Eu(dpa)$_3^{3-}$. Luminescence spectra of Eu(dpa)$_3^{3-}$ in neutral aqueous solution may be assigned to transitions originating from the nondegenerate $^5D_0$ multiplet of the 4f^6(Eu^{3+}) electronic configuration. This multiplet is located at 17 240 cm^{-1} above the $^7F_0$ *ground* multiplet, and a $^5D_0$ luminescence spectrum exhibits six distinct transition regions assigned to $^7F_J \leftarrow {}^5D_0$ (J = 1–6) multiplet to multiplet transition manifolds (the $^7F_0 \leftarrow {}^5D_0$ transition is forbidden in D_3 symmetry). The most intense luminescence is observed in the $^7F_2 \leftarrow {}^5D_0$ and $^7F_4 \leftarrow {}^5D_0$ transition regions, but the strongest chiroptical activity (largest emission dissymmetry) is observed in the $^7F_1 \leftarrow {}^5D_0$ luminescence. In this study, we focus primarily on chiroptical measurements in the $^7F_1 \leftarrow {}^5D_0$ transition region (586–597 nm), with special emphasis on the crystal field component at 594.8 nm.

Two excitation wavelengths were used in the Eu(dpa)$_3^{3-}$ luminescence experiments, 465.8 and 325 nm. Excitation at 465.8 nm produces a $^5D_2$ excited-state population that rapidly decays to the $^5D_0$ emitting level (the $^5D_2$ and $^5D_0$ multiplets are separated by ca. 4210 cm^{-1}). Excitation at 325 nm produces ligand excited states that relax via nonradiative energy transfer to Eu^{3+} (with subsequent population of $^5D_0$).

Quencher Complexes. Among the quencher complexes examined in the present study, Ru(phen)$_3^{2+}$, Ru(bpy)$_3^{2+}$, Co(phen)$_3^{3+}$, and Co(en)$_3^{3+}$, only the ruthenium complexes luminesce. The ruthenium luminescence overlaps the $^7F_1 \leftarrow {}^5D_0$ emission region of Eu(dpa)$_3^{3-}$ and, to a lesser extent, the $^7F_5 \leftarrow {}^5D_4$ emission region of Tb(dpa)$_3^{3-}$. However, the ruthenium luminescence generated by direct radiative excitation has a lifetime at least 3 orders of magnitude shorter than the luminescence lifetimes of either Tb(dpa)$_3^{3-}$ or Eu(dpa)$_3^{3-}$ (in solution with the ruthenium quencher concentrations used in our experiments), and ruthenium luminescence does not interfere with our *time-resolved* measurements of terbium and europium luminescence properties. Weak ruthenium emission *is* observed throughout the time period of Ln* decay, but this emission is from ruthenium complexes excited via Ln* to Ru energy transfer in the quenching processes.

In scanning from long to short wavelengths, the first strong absorption band observed for Ru(phen)$_3^{2+}$ and Ru(bpy)$_3^{2+}$ is centered near 450 nm, with a long-wavelength tail that reaches out to ca. 570 nm. The red side of this band overlaps two terbium emission regions: $^7F_6 \leftarrow {}^5D_4$ (485–495 nm) and $^7F_5 \leftarrow {}^5D_4$ (535–555 nm). However, it does not overlap any europium emission lines. The first strong absorption band observed for Co(phen)$_3^{3+}$ and Co(en)$_3^{3+}$ is centered near 470 nm, with a long-wavelength tail that reaches out to ca. 560 nm. On the basis of spectral overlap considerations alone (within the ruthenium and cobalt absorption regions just mentioned), one may expect that terbium luminescence can be quenched by Tb* → Q energy-transfer processes, whereas europium luminescence cannot be quenched by an analogous Eu* → Q energy-transfer mechanism. However, it is important to note that the cobalt complexes have additional (but very much weaker) absorption bands at longer wavelengths that do overlap europium emission lines (vide infra).

Experimental Section

Preparation of Complexes. Eu(dpa)$_3^{3-}$ and Tb(dpa)$_3^{3-}$. Stock solutions of the two lanthanide complexes were prepared in the same manner. The appropriate lanthanide carbonate, $Eu_2(CO_3)_3$ or $Tb_2(CO_3)_3$, was reacted with 6 equiv of dipicolinic acid in H_2O. The resulting solution was brought to pH 8 with addition of Na_2CO_3, and the solution was diluted to bring the lanthanide concentration to 20 mM.

Transition-Metal Complexes. Ru(phen)$_3$(ClO$_4$)$_2$ was prepared and resolved according to Gillard and Hill,[23] with potassium antimoyl-*d*-tartrate as the resolving reagent. Both enantiomers were recovered from the resolution, and each was recrystallized three times. Optical rotations: Λ-(+)-Ru(phen)$_3^{2+}$ $[\alpha]_D$ = +1389°; Δ-(−)-Ru(phen)$_3^{2+}$ $[\alpha]_D$ = −1319; lit.[24] $|[\alpha]_D|$ = 1340°. Λ-(+)-Ru(bpy)$_3$(ClO$_4$)$_2$ was prepared by dripping a solution of Λ-(+)-Ru(bpy)$_3$I$_2$, a gift of R. A. Palmer (Duke University), into a cold 4 M NaClO$_4$ solution. Optical rotation: Λ-(+)-Ru(bpy)$_3^{2+}$ $[\alpha]_D$ = +805°; lit.[24] $[\alpha]_D$ = +800°. Λ-(+)-Co(en)$_3$Cl$_3$·$^1/_2$NaCl·3H$_2$O was supplied by P. N. Schatz (University of Virginia). Optical rotation: Λ-(+)-Co(en)$_3^{3+}$ $[\alpha]_D$ = +88°; lit.[25] for Λ-(+)-Co(en)$_3$I$_3$ $[\alpha]_D$ = +91°. Δ-(+)-Co(phen)$_3$(ClO$_4$)$_3$ was synthesized by J. P. Bolender (University of Virginia) as a pure enantiomer by the method of Neuman et al.[26] Optical rotation: Δ-(+)-Co(phen)$_3^{3+}$ $[\alpha]_D$ = +824°; lit.[24] $[\alpha]_D$ = +800°. Stock solutions of each transition-metal quencher complex were made up in H_2O, and the concentration of each was determined spectrophotometrically.

Instrumentation and Measurement Techniques. Absorption measurements were made on a Cary 2415 UV/vis/near-IR absorption spectrophotometer. Emission and CPL spectra were recorded on an instrument constructed in our laboratory at the University of Virginia. For excitation, we used a helium–cadmium laser (Liconix 4207NB) for irradiation at 325 nm and an argon ion laser (Coherent Innova 90-6UV) for irradiation at 465.8 (Eu^{3+}) or 488.0 nm (Tb^{3+}). For the time-resolved spectra, the laser output was chopped by a Stanford Research Systems chopper (SR540A) with a laboratory-built narrow two-slot blade. Under typical operation, the chopper was operated at a frequency of 98 Hz and the sample was exposed to laser radiation for 105 μs and blocked from laser radiation for 10 ms.

The sample was held in a water-jacketed 1-cm fluorescence cuvette. The emission was collected at 90° to the excitation direction and passed through a photoelastic modulator (Hinds International PEM-80, operating at a modulation frequency of 50 kHz) and a linear polarizer, which together serve as a circular polarization analyzer. The emission was focused on the entrance slit of a Spex 1400-II $^3/_4$-m monochromator. The dispersed radiation was detected with an EMI 9558 photomultiplier tube, operated in a photon-counting mode. We used a laboratory-built, gated photon-counting device, referenced to the modulation frequency of the PEM, to determine the temporal distribution of the photon pulses, both within the PEM cycle (which determines the CPL content of the emission) and along a train of PEM cycles after the excitation pulse (which determines the decay characteristics of the emission). The temporal resolution of this system is 20 μs, the period of one photoelastic modulator cycle. Details of the construction of the gated photon-counting device will appear elsewhere.[27]

The photon-counting device is interfaced to an AT-clone computer via a high-speed parallel interface (Metrobyte PDMA-16). In order to achieve the large signal to noise ratios required for the observation of small TR-CPL signals, many hundreds of thousands of emission decays are summed. Each time-resolved spectrum reported in this paper represents many hours of data collection time. Sample stability was checked by measuring decay characteristics at both the start and the end of a spectral run.

Data Manipulation and Deconvolution. Of numerical interest in these measurements are determinations of k_0, k_q, k_d, and $g_{em}^{\Delta}(\lambda') = -g_{em}^{\Delta}(\lambda')$ for each quencher–Ln(dpa)$_3^{3-}$ combination. During our time-resolved measurements, we simultaneously acquire $\Delta I(\lambda',t)$ and $I(\lambda',t)$ data from which is calculated $g_{em}(\lambda',t)$ data. As was stated earlier, k_0 and k_q may be determined from $I(\lambda',t)$ measurements for systems containing different concentrations of *racemic* quencher by the fitting equation

$$I(\lambda',t) = I(\lambda',0)e^{-(k_0+k_q[Q])t} + \text{dc} \qquad (40)$$

This equation is derived from eq 26, with η_Q = 0 (racemic quencher) and with the last term being a correction factor for the offset in the measured $I(\lambda',t)$ data created by dark counts (dc). The unquenched Ln(dpa)$_3^{3-}$ lifetime k_0 is determined with no quencher present.

(23) Gillard, R. D.; Hill, R. E. E. *J. Chem. Soc., Dalton Trans.* **1974**, 1217–1236.
(24) McCaffery, A. J.; Mason, S. F.; Ballard, R. E. *J. Chem. Soc.* **1965**, 2883–2892.
(25) Broomhead, J. A.; Dwyer, F. P.; Hogarth, J. W. *Inorg. Synth.* **1960**, *6*, 186–188.
(26) Lee, C. S.; Gorton, E. M.; Neumann, H. M.; Hunt, H. R., Jr. *Inorg. Chem.* **1966**, *5*, 1397–1399.
(27) Metcalf, D. H.; Cummings, W. J.; Richardson, F. S. Manuscript in preparation.

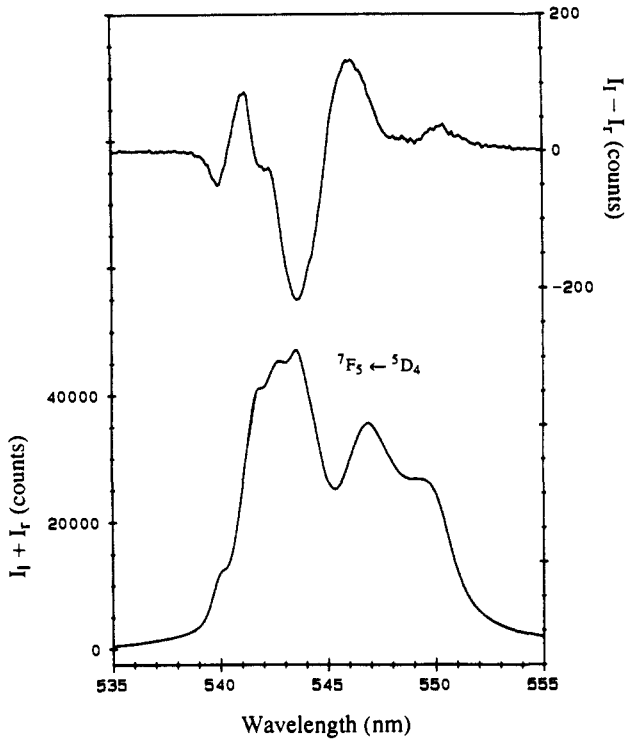

Figure 3. Steady-state TL (lower trace) and CPL (upper trace) spectra recorded in the $^7F_5 \leftarrow {}^5D_4$ (Tb^{3+}) emission region for a solution of Tb-$(dpa)_3^{3-}$ (10 mM) and Λ-Co$(en)_3^{3+}$ (25 μM) in H_2O at 20 °C. Excitation at 488 nm.

Values of $|k_d|$ and $|g_{em}^{\Lambda(\Delta)}(\lambda')|$ are determined by fitting time-resolved dissymmetry data to the equation

$$g_{em}(\lambda',t) = g_{em}^{\Lambda}(\lambda') \tanh\left[\frac{k_d\eta_Q[Q]t}{2}\right]\frac{I(\lambda',t) - dc}{I(\lambda',t)} \qquad (41)$$

This equation is derived from eq 21, with a correction factor for the dark count offset in the $I(\lambda',t)$ data. The dark count correction factor becomes important at long times in the $g_{em}(\lambda',t)$ data, since a significant proportion of the $I(\lambda',t)$ measured (the denominator in the g_{em}^{Λ} calculation) will be dark counts.

The plots of $g_{em}(\lambda',t)$ versus t (Figures 5b, 8b, an 9b, vide infra) should have the appearance of a tanh function, with increasing values of $g_{em}(\lambda',t)$ with increasing t, up to some asymptotic limit, which represents the limiting $g_{em}^{\Lambda(\Delta)}(\lambda')$ value for fully resolved Λ(Δ)-Ln$(dpa)_3^{3-}$ complex. The *slope* of the g_{em} plot is given by the derivative

$$\frac{dg_{em}(\lambda',t)}{dt} = \frac{g_{em}^{\Lambda}(\lambda')k_d\eta_Q[Q]}{2}\,\mathrm{sech}^2\left[\frac{k_d\eta_Q[Q]t}{2}\right] \qquad (42)$$

where sech is the hyperbolic secant function. At small t, the second term will approach 1 and so the slope with be $g_{em}^{\Lambda}(\lambda')k_d\eta_Q[Q]/2$. At large t, the second term approaches 0 and so the g_{em} plot flattens out. Note that, at large values of t, the tanh function in eq 41 approaches 1, and so the limiting $g_{em}^{\Lambda}(\lambda')$ value is reached. Fitting of the early portion of the experimental $g_{em}(\lambda',t)$ plot will lead to well-determined values for the product $k_d g_{em}^{\Lambda}(\lambda')$, while fitting of the latter portion of the experimental data will lead to values of $g_{em}^{\Lambda}(\lambda')$. It is important, therefore, to collect time-resolved dissymmetry data at long t, in order to determine $g_{em}^{\Lambda}(\lambda')$. This can be somewhat difficult, since at long times in the emission decay there is not much emission and noise and dark counts in the data become significant.

We use a Marquardt-based, nonlinear least-squares algorithm for fitting of the data to eqs 40 and 41.[28] The dark count term in each can either be estimated from instrumental characteristics or used as an additional fitting parameter.

Results

General Results. In this section and hereafter we will continue to use an abbreviated notation for the two lanthanide complexes:

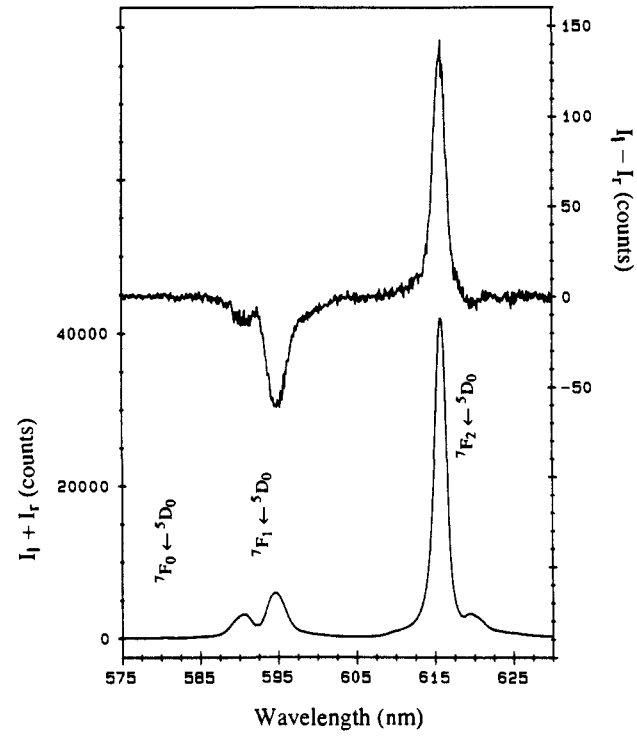

Figure 4. Steady-state TL (lower trace) and CPL (upper trace) spectra recorded in the $^7F_{0-2} \leftarrow {}^5D_0$ (Eu^{3+}) emission region for a solution of Eu$(dpa)_3^{3-}$ (10 mM) and Λ-Co$(en)_3^{3+}$ (25 μM) in H_2O at 20 °C. Excitation at 465.8 nm.

Tb for Tb$(dpa)_3^{3-}$ and Eu for Eu$(dpa)_3^{3-}$. We will also use the generic notation Ln and Q for the lanthanide complexes and quencher species, respectively.

The spectral dispersion characteristics of the total luminescence (TL) measured for the Tb$(dpa)_3^{3-}$ and Eu$(dpa)_3^{3-}$ complexes are not altered by the addition of quencher complexes to a solution sample. Furthermore, the circularly polarized luminescence (CPL) generated by enantioselective quenching exhibits spectral dispersion characteristics identical with those observed in CPL generated by circularly polarized excitation of the Tb and Eu complexes (in the *absence* of any chiral reagents). These results indicate that the TL and CPL observed in our experiments derive entirely from Tb* and Eu* complexes that are free of any perturbations by the transition-metal complexes. The latter complexes act only as excited-state quenchers, thereby reducing the mean luminescence lifetimes and intensities, but not altering spectral dispersion characteristics. Examples of TL and CPL spectra are shown in Figure 3 for the $^7F_5 \leftarrow {}^5D_4$ transition region of Tb* and in Figure 4 for the $^7F_{0-2} \leftarrow {}^5D_0$ transition regions of Eu*. These spectra were obtained for solutions in which [Ln] = 10 mM, [Q] = 25 μM, and the quencher complex was Λ-Co$(en)_3^{3+}$. Note that the largest value of $|g_{em}| = |2\Delta I/I|$ observed in the Tb* spectra is at 543.7 nm and the largest value of $|g_{em}|$ observed in the Eu* spectra is at 594.8 nm. Our time-resolved TL and CPL measurements were carried out at these respective wavelengths.

All four of the transition-metal complexes considered in this study effected partial quenching of Tb* luminescence, and in each case some degree of enantioselectivity was observed in the quenching. On the other hand, only one complex, Co$(en)_3^{3+}$, was an effective quencher of Eu* luminescence. The other three complexes produced no detectable effects on any of the Eu* luminescence properties. Results from our luminescence quenching measurements follow.

Tb$(dpa)_3^{3-}$–Ru$(phen)_3^{2+}$. Time-resolved TL and CPL are shown in Figure 5a for an aqueous solution of Tb$(dpa)_3^{3-}$ (10 mM) and Δ-Ru$(phen)_3^{2+}$ (10 μM) excited at 325 nm. The emission dissymmetry factor data derived from the TR-TL and TR-CPL measurements are displayed in Figure 5b (the noisy trace) along with a plot that represents a fit of the $g_{em}(\lambda',t)$ data to eq 41 (the smooth trace). Steady-state TL and CPL measurements on this

(28) Demas, J. N. *Excited State Lifetime Measurements*; Academic Press: New York, 1983. Marquardt, D. W. *J. Soc. Ind. Appl. Math* **1963**, *11*, 431–441.

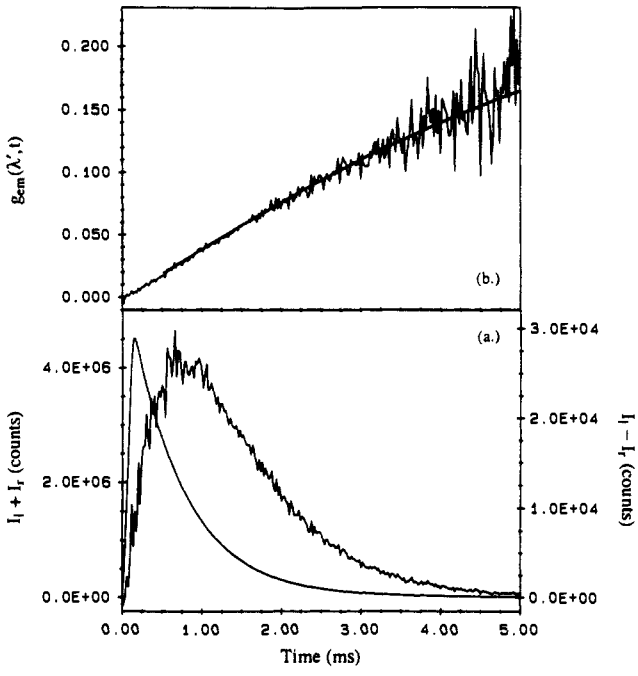

Figure 5. (a) Time-resolved TL (smooth trace, left-hand scale) and CPL (noisy trace, right-hand scale) measured for an aqueous solution of Tb(dpa)$_3^{3-}$ (10 mM) and Δ-Ru(phen)$_3^{2+}$ (10 μM). Excitation was at 325 nm, emission intensity was monitored at 543.7 nm, and the sample temperature was 20 °C. (b) Emission dissymmetry data (noisy trace) evaluated from time-resolved TL and CPL in (a). The smooth trace represents a fit of these data to eq 41 (see text) with $|k_d| = 3.40 \times 10^7$ M^{-1} s^{-1} and $|g_{em}^{\Delta}| = 0.226$.

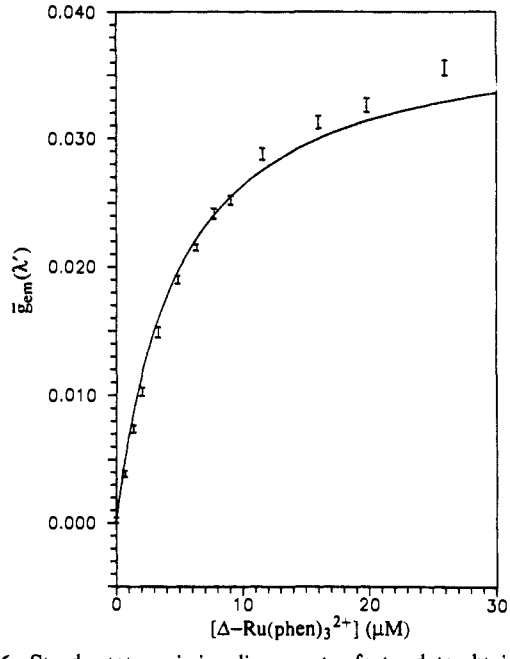

Figure 6. Steady-state emission dissymmetry factor data obtained for Tb(dpa)$_3^{3-}$ (10 mM) in aqueous solution with varying concentrations of Δ-Ru(phen)$_3^{2+}$. The data points (shown with uncertainty bars) are from experiment, and the solid-line plot is calculated from eq 35 (see text) with the appropriate parameters from Table I. Excitation was at 325 nm, emission intensity was monitored at 543.7 nm, and the sample temperature was 20 °C.

sample yielded a value of 2.302×10^{-2} for $\bar{g}_{em}$ (at the emission wavelength $\lambda' = 543.7$ nm). Steady-state measurements performed on samples with a fixed Tb concentration (10 mM) but with different Δ-Ru(phen)$_3^{2+}$ concentrations (between 0 and 28 μM) produced the $\bar{g}_{em}$ data plotted in Figure 6. These data reflect the dependence of $\bar{g}_{em}$ on [Q], as specified by eq 35. Figure 7 shows $\bar{g}_{em}$ data obtained from a series of steady-state measurements

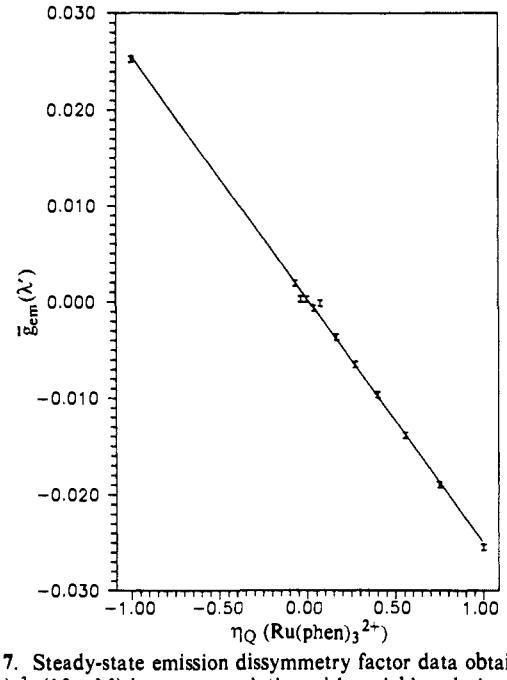

Figure 7. Steady-state emission dissymmetry factor data obtained for Tb(dpa)$_3^{3-}$ (10 mM) in aqueous solution with variable *relative* concentrations of Λ-Ru(phen)$_3^{2+}$ and Δ-Ru(phen)$_3^{2+}$. The *total* concentration of Ru(phen)$_3^{2+}$ was held fixed at 10 μM. The enantiomeric excess parameter η_Q is defined by eq 1 in the text. Excitation was at 325 nm, emission intensity was monitored at 543.7 nm, and the sample temperature was 20 °C. The solid line represents a linear least-squares fit of these data: slope −0.0254, intercept 0.0003.

on samples that contained Tb (10 mM) and variable *relative* amounts of Δ-Ru(phen)$_3^{2+}$ and Λ-Ru(phen)$_3^{2+}$, with the *total* Ru(phen)$_3^{2+}$ concentration fixed at 10 μM. These data reflect the dependence of $\bar{g}_{em}$ on η_Q, the enantiomeric excess in the quencher concentration (see eqs 1 and 35).

All of the data shown in Figures 5–7 were obtained from experiments in which the sample temperature was maintained at 20 °C and sample luminescence was excited with the 325-nm output of a He–Cd CW laser (at power levels less than 5 mW). Under these conditions we found no evidence for photoracemization or photodecomposition of the Ru(phen)$_3^{2+}$ complexes. Analogous experiments were carried out in which sample luminescence was excited with the 488-nm line of a cw argon ion laser. Higher power input was required in these experiments because the absorptivity of Tb(dpa)$_3^{3-}$ is much lower at 488 nm than at 325 nm. Under these conditions (with sample irradiation at 488 nm), the Ru(phen)$_3^{2+}$ complexes undergo slow photoracemization. Results obtained with 488 nm versus 325 nm excitation are essentially identical when 488-nm input power is 100 mW (or less) *and* data collection times are less than 5 min.

The rate parameters determined from analyses of the TL and CPL data of Tb(dpa)$_3^{3-}$–Ru(phen)$_3^{2+}$ are given in Table I, along with the values derived for $|g_{em}^{\Lambda}(\lambda')|$ and $|E_q|$. These results are based entirely on data acquired for solution samples in which [Tb] = 5, 10, or 15 mM, [Q] ranged from 0 to 28 μM, and the temperature was maintained at 20 °C. Recall from our earlier discussion (see Theory and Measurement Methodology) that the *absolute* signs of k_d, E_q, and $g_{em}^{\Lambda}(\lambda')$ cannot be determined from our measurements. However, the sign of $E_q g_{em}^{\Lambda}(\lambda')$, or equivalently $-k_d g_{em}^{\Lambda}(\lambda')$, is determined, and that sign is given in the next to last column of Table I. The quantity shown in the last column of Table I corresponds to *either* $k_q^{\Lambda\Lambda}/k_q^{\Delta\Delta}$ (if $E_q \geq 0$) *or* $k_q^{\Delta\Delta}/k_q^{\Lambda\Lambda}$ (if $E_q \leq 0$), and in later discussion we will refer to this quantity as an *enantiomeric preference ratio.*

Tb(dpa)$_3^{3-}$–Ru(bpy)$_3^{2+}$. Experiments on aqueous solutions of Tb(dpa)$_3^{3-}$–Ru(bpy)$_3^{2+}$ were carried out under conditions analogous to those described above for Tb(dpa)$_3^{3-}$–Ru(phen)$_3^{2+}$. The results obtained from these experiments are summarized in Table I. Note that the value of the k_q rate parameter is only about 17% smaller than that determined for Ru(phen)$_3^{2+}$. However, the value

Table I. Parameter Values Determined from Analyses of CPL and TL Data[a]

Ln*	Q	k_o (s^{-1})	$k_q \times 10^{-7}$ (M^{-1} s^{-1})	$\lvert k_d\rvert \times 10^{-7}$ (M^{-1} s^{-1})	$\lvert g_{em}^{\Lambda}(\lambda')\rvert$[b]	$\lvert E_q\rvert$	sign of $E_q g_{em}^{\Lambda}(\lambda')$	$(1 + \lvert E_q\rvert)/(1 - \lvert E_q\rvert)$[c]
$Tb(dpa)_3^{3-}$	$Ru(phen)_3^{2+}$	469.5	9.86	3.40	0.226	0.17	+	1.41
	$Ru(bpy)_3^{2+}$	469.5	8.24	0.32	0.22	0.02	+	1.04
	$Co(phen)_3^{3+}$	469.5	13.4	5.74	0.22	0.21	+	1.53
	$Co(en)_3^{3+}$	469.5	3.71	0.78	0.22	0.11	+	1.25
$Eu(dpa)_3^{3-}$	$Co(en)_3^{3+}$	619.7	2.98	1.96	0.135	0.33	+	1.99

[a] Parameter definitions are given in Theory and Measurement Methodology. Experimental conditions under which data were obtained for each Ln*-Q system are given in Results. [b] For Tb*, $\lambda' = 543.7$ nm. For Eu*, $\lambda' = 594.8$ nm. [c] This quantity is referred to as an *enantiomeric preference ratio* in the text, and it corresponds to *either* $k_q^{\Delta\Delta}/k_q^{\Lambda\Lambda}$ (if $k_q^{\Delta\Delta} \geq k_q^{\Lambda\Lambda}$) *or* $k_q^{\Lambda\Lambda}/k_q^{\Delta\Delta}$ (if $k_q^{\Lambda\Lambda} \geq k_q^{\Delta\Delta}$).

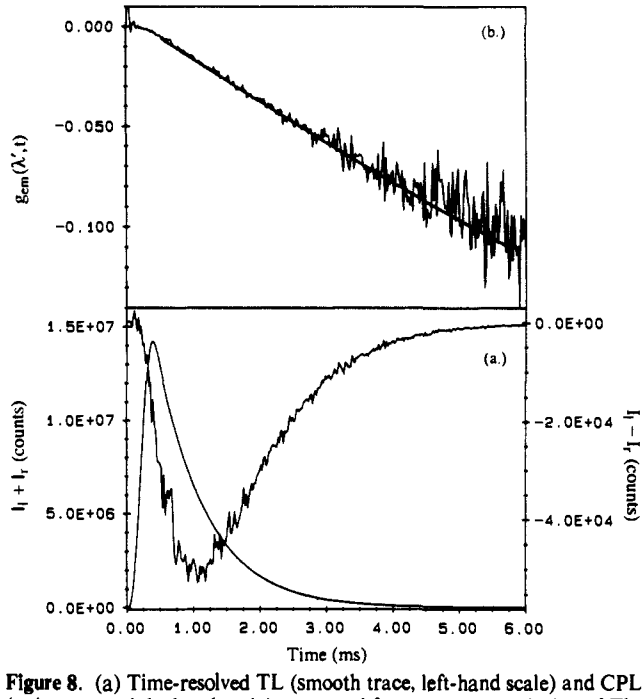

Figure 8. (a) Time-resolved TL (smooth trace, left-hand scale) and CPL (noisy trace, right-hand scale) measured for an aqueous solution of Tb-$(dpa)_3^{3-}$ (10 mM) and Λ-$Co(en)_3^{3+}$ (25 μM). Excitation was at 325 nm, emission intensity was monitored at 543.7 nm, and the sample temperature was 20 °C. (b) Emission dissymmetry data (noisy trace) evaluated from time-resolved TL and CPL in (a). The smooth trace represents a fit of these data to eq 41 (see text) with $|k_d| = 0.78 \times 10^7$ M^{-1} s^{-1} and $|g_{em}^{\Lambda}| = 0.22$.

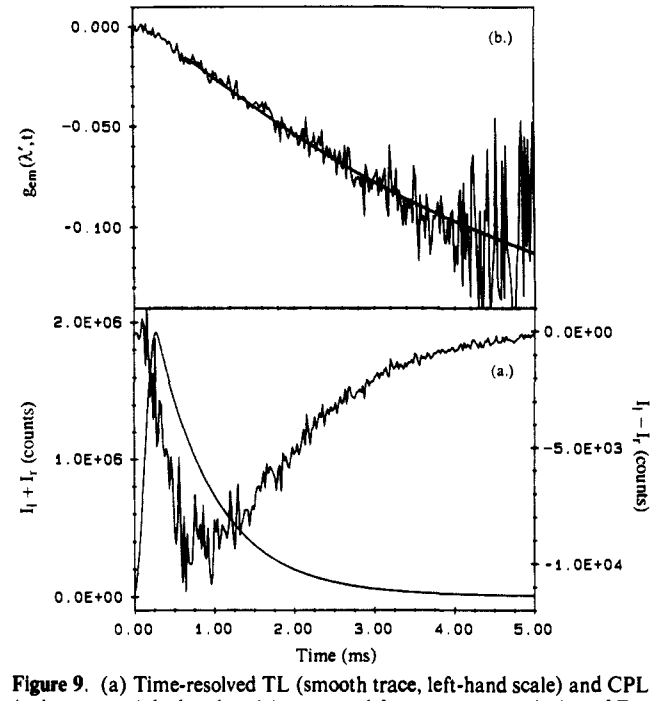

Figure 9. (a) Time-resolved TL (smooth trace, left-hand scale) and CPL (noisy trace, right-hand scale) measured for an aqueous solution of Eu-$(dpa)_3^{3-}$ (10 mM) and Λ-$Co(en)_3^{3+}$ (25 μM). Excitation was at 325 nm, emission intensity was monitored at 594.8 nm, and the sample temperature was 20 °C. (b) Emission dissymmetry data (noisy trace) evaluated from time-resolved TL and CPL in (a). The smooth trace represents a fit of these data to eq 41 (see text) with $|k_d| = 1.96 \times 10^7$ M^{-1} s^{-1} and $|g_{em}^{\Lambda}| = 0.135$.

of $|k_d|$ for $Ru(bpy)_3^{2+}$ is *1 order of magnitude* smaller than that determined for $Ru(phen)_3^{2+}$. The two ruthenium complexes show similar *overall* quenching efficiencies, but $Ru(phen)_3^{2+}$ exhibits a much greater degree of enantioselectivity in its quenching actions.

Tb(dpa)$_3^{3-}$–Co(en)$_3^{3+}$. Time-resolved TL and CPL are shown in Figure 8a for an aqueous solution of $Tb(dpa)_3^{3-}$ (10 mM) and Λ-$Co(en)_3^{3+}$ (25 μM) excited at 325 nm. The emission dissymmetry factor data derived from the TR-TL and TR-CPL measurements are displayed in Figure 8b (the noisy trace), along with a plot that represents a fit of the $g_{em}(\lambda',t)$ data to eq 41 (the smooth trace). Results obtained with 488-nm versus 325-nm excitation were identical. Samples irradiated with 488-nm light showed *no* evidence for photodecomposition or photoracemization of the $Co(en)_3^{3+}$ complexes, and these complexes remained stable under *cw* 325-nm irradiation for several hours and under *chopped* 325-nm irradiation for several days.

The rate parameters determined from analyses of the TL and CPL data of $Tb(dpa)_3^{3-}$–$Co(en)_3^{3+}$ are given in Table I.

Tb(dpa)$_3^{3-}$–Co(phen)$_3^{3+}$. Aqueous solution samples of Tb-$(dpa)_3^{3-}$–$Co(phen)_3^{3+}$ posed photostability problems, and it was not possible to measure *steady-state* TL, CPL, and $\bar{g}_{em}$ versus wavelength spectra for these samples. However, *time-resolved* TL and CPL measurements were feasible when excitation was at 488 nm (with a defocused argon ion laser beam) *and* data collection times were restricted to less than 10 min. The quenching results obtained from these measurements are summarized in Table I. Note that, among the four quencher complexes examined in this study, $Co(phen)_3^{3+}$ gives the largest values of k_q and $|k_d|$.

Eu(dpa)$_3^{3-}$–Co(en)$_3^{3+}$. Time-resolved TL and CPL are shown in Figure 9a for an aqueous solution of $Eu(dpa)_3^{3-}$ (10 mM) and Λ-$Co(en)_3^{3+}$ (25 μM) excited at 325 nm. The emission dissymmetry factor data derived from the TR-TL and TR-CPL measurements are displayed in Figure 9b. Steady-state emission dissymmetry factor data are plotted in Figure 10 for a series of experiments in which Λ-$Co(en)_3^{3+}$ concentrations were varied (between 0 and 64 μM) and the $Eu(dpa)_3^{3-}$ concentration was held constant (10 mM). The solid-line curve shown in Figure 10 represents a fit of the $\bar{g}_{em}$ data to eq 35. The data shown in Figures 9 and 10 were obtained from TL and CPL intensity measurements at $\lambda' = 594.8$ nm (see Figure 4 for TL and CPL spectra of $Eu(dpa)_3^{3-}$ in solution with $Co(en)_3^{3+}$). Results obtained with 465.8-nm versus 325-nm excitation were identical.

The rate parameters and the values of $|g_{em}^{\Lambda}(\lambda')|$ and $|E_q|$ determined for $Eu(dpa)_3^{3-}$–$Co(en)_3^{3+}$ are given in Table I. Comparing the results obtained for Tb–$Co(en)_3^{3+}$ versus Eu–$Co(en)_3^{3+}$, we note that k_q(Eu) is ca. 20% smaller than k_q(Tb). However, the value of $|k_d|$ determined for Eu–$Co(en)_3^{3+}$ is 2.5 times larger than that determined for Tb–$Co(en)_3^{3+}$. Furthermore, we note from Table I that Eu–$Co(en)_3^{3+}$ exhibits more enantioselectivity in its quenching properties than any of the other systems examined in this study. We do not know the sign of E_q, but if we assume, for illustrative purposes, that it is *positive* for Eu–$Co(en)_3^{3+}$, a

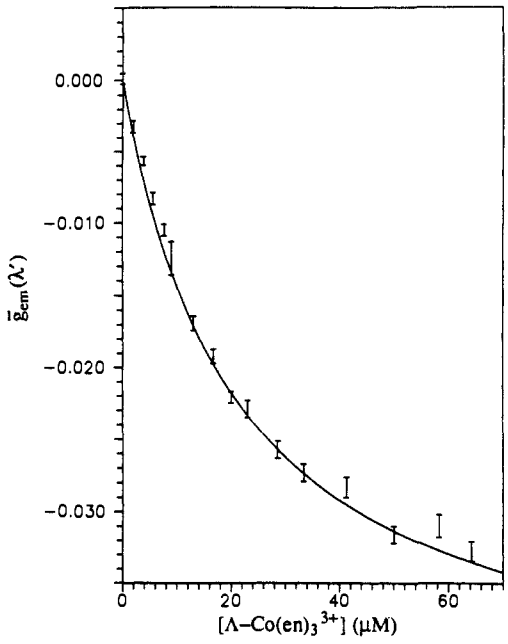

Figure 10. Steady-state emission dissymmetry factor data obtained for Eu(dpa)$_3^{3-}$ (10 mM) in aqueous solution with varying concentrations of Λ-Co(en)$_3^{3+}$. The data points (shown with uncertainty bars) are from experiment, and the solid line plot is calculated from eq 35 (see text) with the appropriate parameters from Table I. Excitation was at 465.8 nm, emission intensity was monitored at 594.8 nm, and the sample temperature was 20 °C.

value of 0.33 for this parameter yields a value of 1.99 for the ratio of $k_q^{\Lambda\Lambda}$ to $k_q^{\Delta\Lambda}$ (see eq 15). If E_q has a *negative* sign, this ratio is 0.50. In either case, there is a 2 to 1 preference of one type of enantiospecific quenching mechanism (homochiral or heterochiral) over the other.

Other Results. All of the results shown in Table I were derived from measurements carried out on samples at 20 °C. Temperature dependence of the rate parameters was not investigated systematically in this study. However, a few measurements were carried out on samples at 4 and 37 °C. At 4 °C, the k_q values are lowered by ca. 10–15% and the $|k_d|$ values are lowered by ca. 8–10% (relative to the respective values at 20 °C); however, the values determined for $|E_q|$ at 4 and 20 °C are essentially the same. From 20 to 37 °C, the k_q values increase slightly (by less than 5%) but the $|k_d|$ values decrease (by 15–20%), indicating less enantioselectivity in the quenching process at the higher temperature. A systematic investigation of temperature-dependent effects is of considerable interest for the processes examined in this study. However, recall from our earlier discussion (see Kinetic Model and Rate Expressions) that *intramolecular* enantiomer interconversion processes within the Ln(dpa)$_3^{3-}$ complexes may be expected to influence our chiroptical observables above ca. 40 °C.[22] These racemization processes within the Ln* excited-state population essentially "undo" part of the excited-state resolution effected by enantioselective quenching, and the k_{conv} terms in expressions 3 and 4 cannot be ignored.

One set of measurements was carried out on Eu(dpa)$_3^{3-}$ and Λ-Co(en)$_3^{3+}$ in D_2O (rather than H_2O). The luminescence lifetime of the Eu* complex is 3.19 ms in D_2O versus 1.61 ms in H_2O (at 20 °C, *without* quencher complex present).[22] However, the values measured for k_q and $|k_d|$ were essentially identical for the D_2O and H_2O solution samples of Eu(dpa)$_3^{3-}$/Λ-Co(en)$_3^{3+}$.

Finally, we report measurements that demonstrate enantioselective interactions between Eu(dpa)$_3^{3-}$ and resolved Ru(phen)$_3^{2+}$. Earlier it was noted that Ru(phen)$_3^{2+}$ does not quench Eu* luminescence, and no CPL is observed for a Eu(dpa)$_3^{3-}$–Λ(or Δ)-Ru(phen)$_3^{2+}$ sample when Eu(dpa)$_3^{3-}$ is excited directly (and selectively). However, when radiative excitation is directly into the ruthenium complex, CPL is observed in both the short-lived Ru* emission *and* in the much longer lived Eu* emission. In this case, Eu* emission is sensitized by Ru* to Eu energy transfer and Eu* CPL reflects chiral discrimination in the energy-transfer mechanism. Accurate rate parameters could not be extracted from these measurements, but *time-integrated* values of g_{em} (λ' = 594.8 nm) were determined: $g_{em} = -1.45 \times 10^{-3}$ (Ru*) and -1.55×10^{-2} (Eu*), for an aqueous solution sample of Δ-Ru(phen)$_3^{2+}$ (73 μM) and Eu(dpa)$_3^{3-}$ (10 mM) at 20 °C.

Discussion

The results obtained in this study provide direct evidence for enantioselective interactions between dissymmetric metal complexes in aqeuous solution. In our experiments, these interactions are between dissymmetric lanthanide complexes in *excited* electronic states (Ln*) and dissymmetric transition-metal complexes in their *ground* electronic state (Q). Enantioselectivity in these interactions is reflected in the differential rates at which ΛLn* and ΔLn* excited states are quenched by resolved (Λ or Δ) Q complexes, and differential (enantioselective) quenching is reflected in the chiroptical properties of the Ln* luminescence. Among the Ln–Q systems examined in this study, we found no evidence for ground-state chiroptical activity in the Ln complexes. Circular dichroism is not observed in the lanthanide absorptive transitions, and circularly polarized luminescence is not observed from *initial* excited-state Ln* populations prepared with unpolarized light. Both the ground-state and initially prepared excited-state populations of lanthanide complexes are racemic, and the generation of chiroptical luminescence with time can be attributed entirely to enantioselective excited-state quenching processes.

The spectral dispersion characteristics of the total luminescence (TL) and circularly polarized luminescence (CPL) observed for Ln* complexes in Ln–Q mixtures (excited with *unpolarized* light) are identical with those observed for the TL and CPL of Ln* complexes in solution *without* quencher, but excited with *circularly polarized* light. These observations indicate that the Q complexes do not perturb the Ln* complexes that survive quenching, and only the k_q and k_d rate parameters in our model will reflect Ln*–Q interactions. The $g_{em}^{\Lambda}(\lambda')$ quantity in our model represents the emission dissymmetry factor of an unperturbed ΛLn* complex (at the emission wavelength λ'), and it may be defined in terms of spectroscopic properties inherent to ΛLn*. For a sample in which the ΛLn* complexes are randomly oriented and emission at λ' is assigned to a transition denoted by e, the emission dissymmetry factor $g_{em}^{\Lambda}(\lambda')$ may be expressed in terms of transition rotatory strengths and dipole strengths as follows[16]

$$g_{em}^{\Lambda}(\lambda') = \frac{4\chi(\lambda')R_e^{\Lambda}}{D_e^{\Lambda}} \tag{43}$$

where R_e^{Λ} denotes a transition rotatory strength, D_e^{Λ} denotes a transition dipole strength, and $\chi(\lambda')$ corrects for sample refractivity effects on the spectroscopic emission processes at wavelength λ'. Defined in terms of *electric* and *magnetic* dipole transition vectors, the rotatory and dipole strengths are given by[16]

$$R_e^{\Lambda} = -i(e_1^{\Lambda}|\hat{\mu}|e_2^{\Lambda})\cdot(e_2^{\Lambda}|\hat{\mathbf{m}}|e_1^{\Lambda}\rangle \tag{44}$$

$$D_e^{\Lambda} = |(e_1^{\Lambda}|\hat{\mu}|e_2^{\Lambda}\rangle|^2 + |(e_1^{\Lambda}|\hat{\mathbf{m}}|e_2^{\Lambda}\rangle|^2 \tag{45}$$

where i is the imaginary number, $\hat{\mu}$ and $\hat{\mathbf{m}}$ denote the electric and magnetic dipole moment operators, respectively, and e_1^{Λ} and e_2^{Λ} label the initial and final states in the emissive transition (e). The analogous expressions for ΔLn* complexes yield the relationships $R_e^{\Delta} = -R_e^{\Lambda}$, $D_e^{\Delta} = D_e^{\Lambda}$, and $g_{em}^{\Delta}(\lambda') = -g_{em}^{\Lambda}(\lambda')$.

The measurements performed in this study yield the magnitude but not the sign of $g_{em}^{\Lambda}(\lambda')$ (see Table I), and this ambiguity in the sign of $g_{em}^{\Lambda}(\lambda')$ precludes our determining the sign of the differential (quenching) rate parameter k_d and the sign of the enantioselectivity parameter E_q. This dilemma cannot be resolved by any kind of solution-phase spectroscopic measurements on the stereochemically labile Ln(dpa)$_3^{3-}$ complexes. This problem can only be solved by growing optical-quality single crystals that contain just one of the Ln(dpa)$_3^{3-}$ enantiomers, determining the absolute configuration of the isolated enantiomer by X-ray crystallographic analysis, and performing chiroptical studies on the structurally characterized crystals. We have not yet succeeded

in our attempts to prepare suitable crystal enantiomorphs that contain resolved $Eu(dpa)_3^{3-}$ or $Tb(dpa)_3^{3-}$.

The k_q and k_d rate parameters determined in this study reflect Ln*–Q interactions that contribute to nonradiative deexcitation (quenching) of the Ln* complexes. The k_q parameter reflects the *average of heterochiral* (ΛLn*–ΔQ or ΔLn*–ΛQ) and *homochiral* (ΛLn*–ΛQ or ΔLn*–ΔQ) interaction contributions, whereas the k_d parameter is defined to reflect the *difference* between heterochiral and homochiral interaction contributions (see eqs 12 and 13). The luminescence measurements performed on the $Tb(dpa)_3^{3-}$–$Ru(phen)_3^{2+}$ and $Tb(dpa)_3^{3-}$–$Ru(bpy)_3^{2+}$ systems give direct evidence that Tb* quenching in these systems occurs via Tb* to Ru electronic energy transfer. The TR-TL spectra show a ruthenium emission component that decays at the same rate as Tb* emission, and this can only be accounted for by a Ru* excited-state population produced by Tb* to Ru electronic energy transfer. Both of the cobalt complexes, $Co(phen)_3^{3+}$ and $Co(en)_3^{3+}$, are effective Tb* quenchers, and each has an electronic state structure and spectroscopic properties suitable for Tb* to Co electronic energy transfer. However, these cobalt complexes are not luminescent, and we have no direct evidence that Co* species (in excited *electronic* states) are formed in the Tb*–Co quenching processes.

It was noted earlier (see Excitation and Emission Properties of Complexes) that each of the transition-metal complexes considered in this study exhibits its first relatively strong absorption band (in scanning from long to short wavelengths) in the blue visible spectral region. In each case, the longer wavelength side of this relatively broad absorption band overlaps *two* Tb* emission manifolds ($^7F_6 \leftarrow {}^5D_4$ and $^7F_5 \leftarrow {}^5D_4$), but the band does *not* overlap *any* of the Eu* emission manifolds, all of which are observed at wavelengths >580 nm. For the ruthenium complexes, this band locates the lowest energy electronic (and vibronic) *acceptor* levels available for Ln* to Ru resonance energy-transfer processes, and these complexes quench Tb* luminescence but not Eu* luminescence. For the cobalt complexes, the blue visible absorption band is centered near 470 nm and is assigned to *spin-allowed* d–d transitions derived from $^1A_{1g} \rightarrow {}^1T_{1g}$ octahedral (O_h) parentage. The *spin-forbidden* d-d transitions derived from $^1A_{1g} \rightarrow {}^3T_{2g}$ and $^1A_{1g} \rightarrow {}^3T_{1g}$ octahedral parentage are expected to give very weak absorptions that span significant parts of the 550–900-nm spectral region, and these transitions will overlap several Tb* *and* Eu* emission manifolds. These transitions have not been characterized for the $Co(en)_3^{3+}$ and $Co(phen)_3^{3+}$ complexes, but they are very well characterized for $Co(NH_3)_6^{3+}$, which has a similar $3d^6(Co^{3+})$ electronic state structure.[29] On the basis of spectral overlap considerations alone, suitable acceptor levels for Tb* to Co energy transfer may derive from the $^1T_{1g}$, $^3T_{2g}$, and $^3T_{1g}$ excited states of $3d^6(Co^{3+})$ and acceptor levels for Eu* to Co energy transfer may derive from the $^3T_{2g}$ and $^3T_{1g}$ excited states. Both the $Co(en)_3^{3+}$ and $Co(phen)_3^{3+}$ complexes quench Tb* luminescence, but only $Co(en)_3^{3+}$ quenches Eu* luminescence (see Table I).

It is not clear why $Co(phen)_3^{3+}$ is *ineffective* as a Eu* quencher but is 3.6 times *more effective* than $Co(en)_3^{3+}$ as a Tb* quencher. The $Co(phen)_3^{3+}$ complex is somewhat larger in size and less regular in shape than $Co(en)_3^{3+}$, and the distance between metal centers in Ln*–$Co(phen)_3^{3+}$ collisions would be greater than in Ln*–$Co(en)_3^{3+}$ collisions (see structures in Figure 2). Therefore, one might argue that exchange interactions between the optical electrons on the two metal centers would be much weaker in Ln*–$Co(phen)_3^{3+}$ compared to those in Ln*–$Co(en)_3^{3+}$, and this would make $Co(en)_3^{3+}$ the more effective acceptor species in a Ln* to Co energy-transfer quenching mechanism. This would explain the Eu*–Co quenching results but not the Tb*–Co quenching results. The differences between these results most likely reflect differences in the donor–acceptor state resonances required to support energy-transfer processes in the respective Ln*–Co systems. Recall that the $^1T_{1g}$, $^3T_{2g}$, and $^3T_{1g}$ states of $3d^6(Co^{3+})$ can provide suitable acceptor levels for Tb* to Co energy transfer, whereas only the $^3T_{2g}$ and $^3T_{1g}$ states can provide acceptor levels for Eu* to Co energy transfer.

(29) Wilson, R. B.; Solomon, E. I. *J. Am. Chem. Soc.* **1980**, *102*, 4085–4095.

Table II. Steady-State Parameters for Enantioselective Quenching[a]

Ln*	Q	η_Q	$\lvert E_q \rvert$	[Q] (μM)	$\lvert \bar{\eta}_{Ln^*} \rvert^b$	$\bar{g}_{em}(\lambda')^c$
$Tb(dpa)_3^{3-}$	$Ru(phen)_3^{2+}$	1	0.172	10	0.116	0.0255
				100	0.164	0.0361
	$Ru(bpy)_3^{2+}$	1	0.019	10	0.012	0.0026
				100	0.018	0.0040
	$Co(phen)_3^{3+}$	1	0.214	10	0.159	0.0350
				100	0.207	0.0455
	$Co(en)_3^{3+}$	1	0.105	10	0.046	0.0101
				100	0.093	0.0205
$Eu(dpa)_3^{3-}$	$Co(en)_3^{3+}$	1	0.329	10	0.107	0.0144
				100	0.272	0.0367

[a] Determined for solution samples (at 20 °C) in which [Ln] = 10 mM and [Q] = 10 *or* 100 μM. [b] See eq 37. [c] See eq 35. For Tb*, λ′ = 543.7 nm. For Eu*, λ′ = 594.8 nm.

Chiral discrimination in the Ln*–Q interactions is demonstrated by the enantioselective quenching results shown in Table I (see the k_d and E_q parameters and the *enantioselective preference ratios*). Results of this kind are novel, and there are no previously reported data with which to make direct comparisons. In Table II we show values for $|\bar{\eta}_{Ln^*}|$ and $\bar{g}_{em}(\lambda')$ relevant to samples that contain 10 mM of either $Tb(dpa)_3^{3-}$ or $Eu(dpa)_3^{3-}$ in solution with ΛQ (at either 10 or 100 μM). These results illustrate the extent to which a relatively small concentration of chiral quencher complexes can induce chiroptical activity in a Ln* population prepared under steady-state, unpolarized excitation conditions. Note that the sign of $\bar{g}_{em}(\lambda'=543.7\text{ nm})$ is the same (i.e., *positive*) for all of the Tb*–ΛQ systems, and, therefore, the sign of $\bar{\eta}_{Ln^*}$ is also the same (though indeterminate) for all of these systems. This shows that all of the ΛQ complexes exhibit the same *qualitative* enantiomeric preference in their quenching of ΛTb* versus ΔTb* complexes. This commonality of enantiomeric preference is also reflected in the enantiomeric preference ratios given in Table I *and* in the signs determined for $E_q g_{em}^{\Lambda}(\lambda')$ (which are also shown in Table I).

Long-range interactions between the negatively charged Ln complexes and positively charged Q complexes examined in this study will be dominated by electrostatic (charge–charge) interactions, but these interactions will not exhibit chiral discrimination. At shorter range (including the intermolecular contact region), dispersion forces may contribute to Ln–Q interactions, and these interactions *do* include chiral discrimination terms, which, to lowest order, reflect simultaneously induced electric *and* magnetic dipole transition moments within the interacting molecules.[1,2,8,10] These *discriminatory* dispersion interactions have a R^{-6} dependence on intermolecular distance (R), and their sign and magnitude depend on products of rotatory strength tensor components (doubly summed over transitions of the two interacting molecules). The differential interaction energy for homochiral versus heterochiral pairs of enantiomers will depend on the relative orientations of the interacting enantiomers, but in general this discriminating energy is expected to be about 2 or 3 orders of magnitude *less* than the *non*discriminating dispersion energy.[8,10] Other short-range electrostatic attractive interactions also include chiral discriminatory terms, but for the trigonal-dihedral (D_3) systems examined in this study, these interactions will be insignificant at (and beyond) the intermolecular contact distance.[8]

On the basis of the considerations given above, it is unlikely that significant chiral discrimination will be reflected in the rate constants associated with the *formation* of homochiral versus heterochiral Ln–Q collisional complexes. This suggests that the enantioselectivity observed in ΛLn* versus ΔLn* excited-state quenching by a chiral ΛQ (or ΔQ) molecule must be attributable to differences in the rate constants that govern Ln* to Q energy transfer in ΛLn*–ΛQ (or ΔLn*–ΔQ) versus ΔLn*–ΛQ (or ΛLn*–ΔQ) quenching actions. These differences in rate constants for energy transfer may reflect *structural* differences between the homochiral and heterochiral collisional complexes *and/or* chiral

discrimination in the *electronic* interaction mechanisms responsible for energy transfer. Structural differences between collisional ΛLn*–ΛQ and ΔLn*–ΛQ diasteromers would be dictated by short-range attractive and repulsive (steric) interactions that govern the metal–metal separation distance *and* the relative orientations of the constituent Ln* and Q molecules in a collisional complex. Relative energy-transfer rates would be influenced by both of these structural factors (metal–metal distance *and* relative orientations of the interacting Ln* and Q molecules). Outside the intermolecular contact range, average separation distances for ΛLn*–ΛQ and ΔLn*–ΛQ pairs are expected to be essentially identical, and enantioselective energy transfer at these distances requires a mechanism in which chiral discrimination is *inherent* in the donor–acceptor electronic interactions. For example, in energy-transfer mechanisms based on multipole–multipole (Coulombic) interactions between chiral donor and acceptor systems, chiral discrimination may occur in interactions mediated by circularly polarized (virtual) photons.

The results obtained in this study do not yield definitive information regarding the mechanistic details of energy transfer in the Ln*–Q systems. However, given the relatively small transition densities associated with the relevant donor (Ln*) and acceptor (Q) electronic transitions, it is highly likely that an *electron-exchange* mechanism makes the dominant contribution. This is especially true for the Eu*–$Co(en)_3^{3+}$ system in which the acceptor transitions are spin-forbidden d–d transitions with very small oscillator strengths. The donor and acceptor transitions relevant to resonance energy-transfer processes in the Tb*–Ru and Tb*–Co systems have somewhat larger optical transition densities, but even in these cases it is likely that an electron-exchange mechanism makes larger contributions than multipole–multipole (Coulombic) interaction mechanisms. Expressed in its simplest phenomenological form, the rate constant for energy transfer via an electron-exchange mechanism is given by[30]

$$k_{ex}(R) = k_{ex}^0 e^{-2R/L} \tag{46}$$

where R is the distance between donor and acceptor centers, L is defined as the effective *average* Bohr radius of the excited and unexcited states of the donor and acceptor, and k_{ex}^0 is defined to contain all the details of the relevant electron-exchange interactions and the densities of donor and acceptor states that satisfy resonance conditions. If we define R_0 to be the donor–acceptor separation distance at which the rate constant for energy transfer equals the rate constant for donor excited-state decay (in the absence of acceptor molecules), then $k_{ex}(R_0) = 1/\tau_0$ and eq 46 may be rewritten as

$$k_{ex}(R) = \frac{1}{\tau_0} e^{2R_0/L} e^{-2R/L} \tag{47}$$

where τ_0 denotes the donor excited-state lifetime in the absence of energy transfer and R_0 now reflects the interaction details previously incorporated in the k_{ex}^0 parameters of eq 46.

It is convenient to examine chiral discrimination in the electron-exchange energy-transfer mechanism by considering the ratio

$$r_{ex} = \frac{k_{ex}^{\Lambda\Lambda}}{k_{ex}^{\Delta\Lambda}} = e^{2(R_0^{\Lambda\Lambda} - R_0^{\Delta\Lambda})/L} e^{-2(\bar{R}^{\Lambda\Lambda} - \bar{R}^{\Delta\Lambda})/L} \tag{48}$$

where the ΛΛ and ΔΛ superscripts refer, respectively, to homochiral and heterochiral donor–acceptor pairs, $\bar{R}^{\Lambda\Lambda}$ and $\bar{R}^{\Delta\Lambda}$ are *average* donor–acceptor separation distances in the two types of diastereomeric pairs, and the $R_0^{\Lambda\Lambda}$ and $R_0^{\Delta\Lambda}$ quantities have the same definition as R_0 in eq 47. Different values for $R_0^{\Lambda\Lambda}$ and $R_0^{\Delta\Lambda}$ would imply chiral discriminatory contributions to the electron-exchange integrals associated with the donor–acceptor excited states involved in energy transfer, whereas different values for $\bar{R}^{\Lambda\Lambda}$ and $\bar{R}^{\Delta\Lambda}$ would reflect chiral discrimination in the contact interactions that determine how close the donor and acceptor molecules can get to one another in a collisional complex. If we assume that the enantioselective quenching results obtained in this study derive entirely from chiral discrimination in an electron-exchange energy-transfer quenching mechanism, then eqs 15 and 48 may be combined to obtain the following relationship

$$\frac{k_q^{\Lambda\Lambda}}{k_q^{\Delta\Lambda}} = r_{ex} = e^{2\delta R_0/L} e^{-2\delta\bar{R}/L} = \frac{1 + E_q}{1 - E_q} \tag{49}$$

$$E_q = \frac{e^{2(\delta R_0 - \delta\bar{R})/L} - 1}{e^{2(\delta R_0 - \delta\bar{R})/L} + 1} \tag{50}$$

where $\delta R_0 = R_0^{\Lambda\Lambda} - R_0^{\Delta\Lambda}$, $\delta\bar{R} = \bar{R}^{\Lambda\Lambda} - \bar{R}^{\Delta\Lambda}$, and E_q is defined according to eq 13. It is useful to further rearrange these expressions to obtain

$$\frac{|\delta R_0 - \delta\bar{R}|}{L} = \tfrac{1}{2} \ln\left[\frac{1 + |E_q|}{1 - |E_q|}\right] \tag{51}$$

Note that $\delta R_0 > 0$ corresponds to a preference of homochiral over heterochiral energy transfer via chiral discrimination in the excited-state electron-exchange interactions, whereas $\delta\bar{R} > 0$ implies that the heterochiral collisional complexes are "tighter" or smaller than the homochiral complexes (on average), and this will favor heterochiral over homochiral energy transfer.

Table III. Chiral Discrimination Parameters Based on an Electron-Exchange Mechanism for Ln* to Q Energy Transfer[a]

Ln*–Q	$\lvert\delta R_0 - \delta\bar{R}\rvert/L$	L (Å)	$\lvert\delta R_0 - \delta\bar{R}\rvert$ (Å)
Tb*–$Ru(phen)_3^{2+}$	0.172	2.0	0.344
Tb*–$Ru(bpy)_3^{2+}$	0.0196	2.0	0.039
Tb*–$Co(phen)_3^{3+}$	0.213	1.5	0.319
Tb*–$Co(en)_3^{3+}$	0.112	1.0	0.112
Eu*–$Co(en)_3^{3+}$	0.344	1.0	0.344

[a] See eq 51 and preceding discussion in the text.

The right-hand side of eq 51 can be evaluated from the data given in Table I, and the results are shown in Table III. These results are combined with rough estimates for the L parameter values to obtain approximate values for $|\delta R_0 - \delta\bar{R}|$ (also shown in Table III). The *relative* values chosen for L are intended to reflect differences between the MLCT excited (acceptor) states of the ruthenium complexes and the d–d excited (acceptor) states of the cobalt complexes. The results given in Table III permit some interesting comparisons to be made, but they certainly cannot support *definitive* conclusions regarding the mechanistic or structural origins of chiral discrimination in the systems examined here. However, some general comments are in order. First we note that the results cannot be rationalized in terms of structural discrimination alone. This is most evident in comparing the results for Tb*–$Co(en)_3^{3+}$ and Eu*–$Co(en)_3^{3+}$, which are expected to form essentially isostructural collision complexes with identical (or very similar) values of $\delta\bar{R}$. This suggests that the dramatic difference between the $|\delta R_0 - \delta\bar{R}|$ values obtained for these two systems resides in δR_0. The comparative results obtained for Tb*–$Ru(phen)_3^{2+}$ and Tb*–$Ru(bpy)_3^{2+}$ also indicate a dominant role for δR_0 in enantioselective energy transfer. These systems are not isostructural, but their structural differences are not large enough to rationalize an *order of magnitude* difference in $\delta\bar{R}$ values. On the other hand, the comparative results obtained for Tb*–$Co(phen)_3^{3+}$ and Tb*–$Co(en)_3^{3+}$ are quite compatible with a predominantly structural contribution to $|\delta R_0 - \delta\bar{R}|$. Steric constraints within $Tb(dpa)_3^{3-}$–$Co(phen)_3^{3+}$ pair complexes would be significantly greater than those in $Tb(dpa)_3^{3-}$–$Co(en)_3^{3+}$ complexes (reflecting the relative sizes of the phen and en ligands), and our results suggest that these constraints include significant enantiospecificity. Finally we note that the nearly isostructural Tb*–$Ru(phen)_3^{2+}$ and Tb*–$Co(phen)_3^{3+}$ systems show very similar values for $|\delta R_0 - \delta\bar{R}|$.

The foregoing discussion of our empirical enantioselective quenching data within the context of a phenomenological model for energy transfer (via an electron-exchange mechanism) must be considered highly speculative. A similarly crude phenomenological analysis of the data can be carried out within the context

(30) Dexter, D. L. *J. Chem. Phys.* **1953**, *21*, 836–850.

of a multipole–multipole interaction model for energy transfer (including electric–electric *and* electric–magnetic coupling contributions), but the results are no more informative regarding the structural and mechanistic details of chiral discrimination in the systems examined here. However, one very important (albeit qualitative) conclusion emerges from both types of analyses: chiral discrimination occurs in both homochiral versus heterochiral structural differences *and* excited-state electronic interaction mechanisms. Intermolecular chiral discrimination (or recognition) based on relative molecular size and shape (i.e., stereochemical structure) is a very common and often-used concept in chemistry and biology, and this kind of chiral discrimination is easy to visualize in many systems. Quite often one only needs to examine space-filling molecular models to rationalize enantiomer interaction preferences. However, chiral discrimination in purely electronic interactions (at any given distance) is a somewhat more subtle concept, and its consideration has been limited, in large part, to theory and calculations. Furthermore, the calculations have focused almost entirely on discrimintory *ground-state* interaction energies, and results from these calculations are generally compared to thermodynamic data available for the relevant systems. The enantioselective excited-state quenching data obtained in the present study provide a much more *direct* measure of chiral discriminatory interactions at the *molecular* level, and the quenching rate constants exhibit a higher degree of enantioselectivity than is commonly found in differential thermodynamic properties. The E_q parameters defined and characterized in this study pose useful and interesting challenges for further theory development and refinement. However, significant advances in theory and understanding (beyond the phenomenological level) will require additional experimental studies on a wider variety of systems to (1) help clarify the mechanistic details of the quenching processes, (2) differentiate between structure effects and electronic effects, and (3) assess the importance of environmental factors and sample conditions (including sample temperature and solvent).

Conclusion

Chiroptical luminescence spectroscopy provides a direct probe of excited-state chiroptical activity in molecular systems, and in a recent study we demonstrated how *time-resolved* circularly polarized luminescence (TR-CPL) measurements can be used to investigate *intramolecular* excited-state dynamics in a chiral system.[22] In the present study, we have shown that TR-CPL measurements also provide a very sensitive means for investigating chiral discrimination in *intermolecular*, excited-state quenching processes. Measurement techniques and data analysis schemes are presented for the general case in which opposite enantiomers within an excited-state population of dissymmetric luminophore molecules are differentially quenched by a nonracemic population of dissymmetric quencher molecules. Specific applications are described for the case in which differential, enantioselective quenching generates enantiomeric excess in an initially racemic excited-state population of luminophores. Generation of excited-state enantiomeric excess is monitored by time-resolved emission dissymmetry factor measurements, and the data from these measurements may be used to determine differential rate constants for homochiral versus heterochiral (enantioselective) quenching. Experimental results are reported for a series of luminophore–quencher systems in which quenching occurs via an electronic energy-transfer mechanism, and *enantioselective* quenching may be attributed to chiral discrimination in the luminophore–quencher interactions that govern energy-transfer rates.

Each of the lanthanide (luminophore) and transition-metal (quencher) complexes examined in this study has a tris(chelate) structure in which the metal–ligand chelate rings form a three-bladed propellor with either left-handed (Λ) or right-handed (Δ) helicity about a trigonal symmetry axis. However, two different metal ions (Ru^{2+} and Co^{3+}) and three different ligands (of different size, shape, and electronic structure) are represented among the quencher (Q) complexes, and two different lanthanide luminophores are used, $Eu(dpa)_3^{3-}$ and $Tb(dpa)_3^{3-}$. Therefore, the various pairwise combinations of Ln and Q complexes exhibit significant variability with respect to their *relative* spectroscopic and structural properties. It is expected that this variability will be reflected in the quenching rate parameters determined for the different Ln*–Q systems, and the results given in Table I show variations in the total (*achiral*) quenching rate constants (k_q) *and* in the differential (*chiral discriminatory*) quenching rate parameters (k_d). However, the variations in k_q and $|k_d|$ values differ, both qualitatively and quantitatively, which indicates that the k_q and k_d parameters are sensitive to different aspects of the relative electronic and stereochemical properties of the Ln* and Q partners involved in quenching. The most striking variations between systems are seen in the enantioselectivity parameters (E_q) and in the related enantiomeric preference ratios (see the last column of Table I). The comparative results for Tb^*–$Ru(phen)_3^{2+}$ versus Tb^*–$Ru(bpy)_3^{2+}$ and for Tb^*–$Co(en)_3^{3+}$ versus Eu^*–$Co(en)_3^{3+}$ are particularly striking. The singularly most interesting (and curious) results are those obtained for Eu^*–$Co(en)_3^{3+}$. This system gives the smallest quenching rate constant (k_q), but it exhibits by far the largest degree of enantioselectivity in its quenching processes. The relatively small k_q value is easily rationalized in terms of the respective $Eu(dpa)_3^{3-}$ and $Co(en)_3^{3+}$ electronic state structures, which are not well-matched for Eu* to Co resonance energy transfer. However, the large $|E_q|$ value and enantiomeric preference ratio (nearly 2/1) obtained for this system are difficult to explain, especially when they are compared to the corresponding results for the isostructural Tb^*–$Co(en)_3^{3+}$ system. A similar dilemma is encountered in a comparison of the enantioselectivity results obtained for the Tb^*–$Ru(phen)_3^{2+}$ and Tb^*–$Ru(bpy)_3^{2+}$ systems. The $|E_q|$ values for these systems differ by almost 1 order of magnitude, whereas their k_q quenching constants differ by less than 20%.

The results reported here given direct evidence for chiral discrimination in dynamic, intermolecular energy-transfer processes, and they pose new and interesting challenges for mechanistic interpretations of chiral discrimination in intermolecular interactions. In our discussion of experimental results, we considered enantioselective quenching within the context of a phenomenological model for energy transfer via an electron-exchange mechanism and we developed expressions that relate the enantioselective quenching parameter E_q to a set of parameters inherent to the energy-transfer model (see eqs 49–51). The differential parameters ($\delta\bar{R}$ and δR_0) appearing in these expressions reflect (1) structural differences between the collisional complexes formed by homochiral versus heterochiral diastereomeric donor (Ln*)–acceptor (Q) pairs and/or (2) chiral discrimination in the purely electronic interactions *directly* responsible for energy transfer (i.e., chirality dependence in the electron-exchange integrals). Our results are not sufficient for performing quantitative assessments and drawing definitive conclusions regarding the relative importance of structural versus electronic factors in enantioselective quenching, but qualitative and semiquantitative comparisons of the results obtained for different systems strongly suggest that both types of factors can make important contributions.

Finally, we note that the measurement techniques described in this work provide a very sensitive means for determining enantiomeric excess (or the degree of enantiomeric resolution) in a sample of dissymmetric quencher molecules. The requirements for making this type of determination are apparent from an inspection of eq 35a. The steady-state emission dissymmetry factor of the luminophore, $\bar{g}_{em}(\lambda')$, is directly proportional to quencher enantiomeric excess (η_Q), with a proportionality constant equal to $^1/_2 g^{\Lambda}_{em}(\lambda')k_d[Q]/(k_0 + k_q[Q])$. For any given luminophore–quencher system, this proportionality constant can be evaluated from time-resolved TL and CPL data obtained for a sample of *known* quencher concentration *and* enantiomeric composition, and eq 35a may then be used to determine η_Q for samples of *unknown* enantiomeric composition from *steady-state* emission dissymmetry measurements. Alternatively, this same type of determination can be made from *time-resolved* emission dissymmetry measurements (see eq 21) after the magnitudes and relative signs of $g^{\Lambda}_{em}(\lambda')$ and k_d have been determined for the luminophore–quencher of interest. As an illustration of η_Q determination from

steady-state emission dissymmetry measurements, consider a sample that contains 10 mM of $Tb(dpa)_3^{3-}$ as the racemic probe luminophore and 10 μM of $Ru(phen)_3^{2+}$ quencher (for which η_Q is unknown). With use of the data given in Table I for this system, eq 35a may be evaluated to yield $\bar{g}_{em}(\lambda' = 543.7\ nm) = -2.64 \times 10^{-2}\eta_Q$. The detection limit on the magnitude of $\bar{g}_{em}$ (for Tb* emission at 543.7 nm) is approximately 10^{-4}, and therefore, $|\eta_Q|$ values as small as 0.004 may be determined. This lower limit of $|\eta_Q|$ corresponds to 0.4% enantiomeric (or optical) purity, and in a 10 μM concentration of $Ru(phen)_3^{2+}$ quencher, it corresponds to a 0.04 μM *difference* in the concentrations of the Λ and Δ enantiomers. Applications of enantioselective quenching measurements to the determination of enantiomeric purities will be presented in greater detail in a future report.

Acknowledgment. This work was supported by grants from the National Science Foundation (CHE-8820180 to F.S.R. and CHE-8817809 to J.N.D.). We also gratefully acknowledge many helpful discussions with Dr. James P. Riehl (University of Missouri—St. Louis), essential technical assistance from William J. Cummings, and synthetic efforts of James P. Bolender.

Registry No. $Tb(dpa)_3^{3-}$, 38682-37-0; $Eu(dpa)_3^{3-}$, 38721-36-7; $Ru(phen)_3^{2+}$, 22873-66-1; $Ru(bpy)_3^{2+}$, 15158-62-0; $Co(phen)_3^{3+}$, 18581-79-8; $Co(en)_3^{3+}$, 14878-41-2.

Displacement of CO Chemisorbed on Metals by Hydrogen

John L. Gland,* Daniel A. Fischer, Shikong Shen, and Francisco Zaera

Contribution from the Exxon Research and Engineering Company, Clinton Township, Annandale, New Jersey 08801. *Received July 5, 1988*

Abstract: Chemisorbed CO can be displaced from both the Ni(100) and Pt(111) surfaces by hydrogen in a temperature range where thermally activated desorption is substantially slower. This result is unexpected since hydrogen is adsorbed more weakly than CO on both the Pt and Ni surfaces. This paper describes a series of experiments that clearly establish that *displacement* occurs on these two surfaces. *Displacement* of a strongly adsorbed species by a more weakly adsorbed species is a different process than surface *exchange* where one isotopic form of an adsorbed species is exchanged by another. The kinetic results presented here indicated that the displacement reaction is thermally activated and that the thermal activation barrier is substantially smaller than the thermal activation energy required for CO desorption in the absence of hydrogen. The first-order dependence on surface CO coverage suggests that a single adsorbed CO molecule is involved in the rate-limiting step. The positive order (about 0.5) observed in hydrogen pressure suggests that the atomic hydrogen coverage plays a role in the rate-limiting step. No isotope effect is observed with deuterium substitution. He, Ne, Ar, N_2, and CH_4 do not cause displacement under the conditions studied (up to 10^{-3} Torr). Adsorbed hydrogen is rapidly displaced by CO as expected since hydrogen is more weakly adsorbed than CO. The reaction energetics and probabilities observed are consistent with substantial weakening of adsorbed CO by high coverages of coadsorbed hydrogen.

Carbon monoxide has been studied extensively on both the Ni(100)[1-4] and Pt(111)[5-9] surfaces. CO is adsorbed in terminal and bridge sites on both surfaces; heats of CO adsorption are 30 kcal/mol on the Ni(100) surface[4] and 31 kcal/mol on the Pt(111) surface at low coverages.[6-9] Increasing repulsive interactions between adsorbed CO molecules results in decreasing heats of adsorption with increasing CO coverage on both surfaces. Hydrogen has a heat of adsorption of 23 kcal/mol on the Ni(100) surface[10,11] and about 19 kcal/mol on the Pt(111) surface.[12] The interaction between coadsorbed hydrogen and CO is quite complex on the Ni(100) surface.[13-16] CO adsorbed on a hydrogen-presaturated surface desorbs at about 210 K, about 100 K lower than CO desorption from the clean surfaces; this suggests that a weakened CO–Ni interaction can occur in the presence of a large amount of coadsorbed hydrogen. A recent detailed study of coadsorbed CO and hydrogen on the Pt(111) surfaces indicates that only small repulsive interactions are observed at high coverage. This repulsion results in the formation of CO islands in the presence of hydrogen even for low CO coverages.[17]

Several authors have characterized isotopic exchange of CO and adsorbed atomic hydrogen on metal surfaces.[18,19] Several mechanisms have been proposed to rationalize isotopic exchange which involves weakly adsorbed surface intermediates induced by high adsorbed coverages or resonant energy transfer between incoming molecules and adsorbed molecules. Exchange mechanisms are generally not appropriate for the displacement reactions discussed in this paper.

* Address correspondence to this author at the Department of Chemistry, University of Michigan, Ann Arbor, Michigan 48109.

These experiments were performed in a UHV system described in detail previously[18] equipped with facilities for multiple-mass temperature-programmed desorption, Auger electron spectroscopy

(1) Tracy, J. C. *J. Chem. Phys.* **1971**, *56*, 2736.
(2) Anderson, S. *Solid State Commun.* **1977**, *21*, 75.
(3) Mitchell, G. E. M.; Gland, J. L.; White, J. M. *Surf. Sci.* **1983**, *131*, 167.
(4) Christmann, K.; Schober, O.; Ertl, G.; Neumann, M. *J. Chem. Phys.* **1974**, *60*, 4528.
(5) Froitzheim, H.; Hopster, H.; Ibach, H.; Lehwald, S. *Appl. Phys.* **1977**, *13*, 147.
(6) Ertl, G.; Neumann, M.; Streit, R. M. *Surf. Sci.* **1977**, *64*, 393.
(7) Krebs, H. J.; Lüth, H. *Appl. Phys.* **1977**, *14*, 337.
(8) McCabe, R. W.; Schmidt, L. D. *Surf. Sci.* **1977**, *66*, 101.
(9) Poelsema, B.; Palmer, R. L.; Comsa, G. *Surf. Sci.* **1984**, *136*, 1.
(10) Lapujoulade, J.; Neil, K. S. *Surf. Sci.* **1973**, *35*, 288.
(11) Anderson, S. *Proc. Int. Vac. Congr.*, 7th Int. Conf. Solid Surfaces, 3rd, Vienna, 1977; p 1019.
(12) Poelsema, B.; Mechterscheimer, G.; Comsa, G. *Surf. Sci.* **1981**, *111*, 519.
(13) Goodman, D. W.; Yates, J. T., Jr.; Madey, T. E. *Surf. Sci.* **1980**, *93*, L135.
(14) Koel, B. E.; Peebles, D. E.; White, J. M. *Surf. Sci.* **1981**, *107*, L367.
(15) Koel, B. E.; Peebles, D. E.; White, J. M. *Surf. Sci.* **1983**, *127*, 709.
(16) Koel, B. E.; Peebles, D. E.; White, J. M. *Surf. Sci.* **1983**, *125*, 739.
(17) Bernasek, S. L.; Lenz, K.; Poelsema, B.; Comsa, G. *Surf. Sci.* **1987**, *183*, L319.
(18) Zaera, F.; Fischer, D. A.; Shen, S.; Gland, J. L. *Surface Science* **1988**, *194*, 205.
(19) Gland, J. L.; Shen, S.; Zaera, F.; Fischer, D. A. *J. Vac. Sci. Technol.* **1988**, *A6*, 2426.
(20) Shen, S.; Zaera, F.; Fischer, D. A.; Gland, J. L. *J. Chem. Phys.* **1988**, *89*, 590.

0002-7863/90/1512-5695$02.50/0